Antimicrobial activity of iron-depriving pyoverdines against human opportunistic pathogens

Vera Vollenweider[1], Karoline Rehm[2], Clara Chepkirui[3], Manuela Pérez-Berlanga[1], Magdalini Polymenidou[1], Jörn Piel[3], Laurent Bigler[2], Rolf Kümmerli[1]

[1]Department of Quantitative Biomedicine, University of Zurich, Zurich, Switzerland

[2]Department of Chemistry, University of Zurich, Zurich, Switzerland

[3]Institute of Microbiology, Eidgenössische Technische Hochschule (ETH) Zurich, Zurich, Switzerland

Short title: Pyoverdines against pathogens

Corresponding author: Rolf Kümmerli, Department of Quantitative Biomedicine, University of Zurich, Winterthurerstrasse 190, 8057 Zurich, Switzerland.

Email: rolf.kuemmerli@uzh.ch / Phone: +41 44 635 48 01

Abstract

The global rise of antibiotic resistance calls for new drugs against bacterial pathogens. A common approach is to search for natural compounds deployed by microbes to inhibit competitors. Here we show that the iron chelating pyoverdines, siderophores produced by environmental *Pseudomonas* spp., have strong antibacterial properties by inducing iron starvation and growth arrest in pathogens. A screen of 320 natural *Pseudomonas* isolates used against 12 human pathogens uncovered five pyoverdines with particularly high antibacterial properties and distinct chemical characteristics. The most potent pyoverdine effectively reduced growth of the pathogens *Acinetobacter baumannii*, *Klebsiella pneumoniae* and *Staphylococcus aureus* in a concentration- and iron-dependent manner. Pyoverdine increased survival of infected *Galleria mellonella* host larvae, and showed low toxicity for the host, mammalian cell lines, and erythrocytes. Furthermore, experimental evolution combined with whole-genome sequencing revealed reduced potentials for resistance evolution compared to an antibiotic. Thus, pyoverdines from environmental strains could become new sustainable antibacterials against human pathogens.

Introduction

There are approximately 4.95 million fatalities associated with antibiotic-resistant bacteria worldwide each year[1]. This high mortality rate contrasts with the low development rate of new antibacterial agents for clinical applications[2,3]. Thus, the development of alternative therapies with higher sustainability to counteract the rapidly dwindling treatment options due to resistance evolution is imperative[4–6]. Numerous alternative approaches have been proposed including phage therapy, antimicrobial peptides and nanobodies, anti-virulence treatments to disarm pathogens, treatments that capitalize on ecological competition between susceptible and resistant bacteria, and the search for new antibacterial compounds produced by environmental microbes[7–12].

Mining natural microbial communities has become a promising endeavour in the hunt for novel antimicrobials because most microbes deploy bioactive compounds to contend with their competitors in the diverse assemblies they live in[13]. Competition often involves the secretion of secondary metabolites with specific antimicrobial properties against other microbes[14]. The isolation, characterization and synthesis of such secondary metabolites can result in novel prospective antibiotics for clinical applications[15,16]. Secondary metabolites that act as toxins to kill competitors are often considered promising candidates. However, microbes compete through a variety of mechanisms other than toxins. For example, there is increasing evidence that competition for iron is a main determinant of species interactions in soil and freshwater communities[17,18]. Competition for iron involves the secretion of siderophores, a class of secondary metabolites that scavenges environmental iron with high affinity[19]. Because siderophores are often species specific, they have two opposing effects: they make iron available for related community members

possessing the matching receptor but withhold iron from competitors with non-matching receptors. Thus, siderophores can be competitive agents in inter-species interactions[20–23].

Here, we apply the concept of siderophore-mediated iron competition observed in natural communities to human opportunistic pathogens. Specifically, we investigate whether siderophores from non-pathogenic environmental bacteria can induce iron starvation and growth arrest in human pathogens. We focus on pyoverdines, a class of siderophores with high iron affinity that are produced and secreted by fluorescent *Pseudomonas* spp. under iron-limited conditions[24]. Upon complexation with ferric iron, the iron-loaded pyoverdine is imported into the cell by receptors with high specificity and subsequently reduced to the bio-available ferrous iron[25,26]. Pyoverdines show an extraordinary structural diversity with more than 70 described variants that differ in their peptide backbone[27,28], and have an extremely high affinity for iron ($K_a = 10^{32}$ M^{-1}, pyoverdine produced by *Pseudomonas fluorescens* biotype B)[29]. For these reasons, we propose that pyoverdines from non-pathogenic *Pseudomonas* spp. could be potent agents to reduce the growth of opportunistic human pathogens by intensifying iron competition.

To test our hypothesis, we screened pyoverdines from a library of 320 environmental *Pseudomonas* strains, isolated from soil and freshwater habitats, for their activity against 12 strains of human opportunistic bacteria. For the most promising pyoverdine candidates, we elucidated the chemical structure to assess diversity and to understand the chemical properties important for iron competition. Subsequently, we assessed the efficacy of the three top pyoverdine candidates against four human opportunistic pathogens (*Acinetobacter baumannii*, *Klebsiella pneumoniae*, *Pseudomonas aeruginosa* and *Staphylococcus aureus*) *in vitro* and/or

in vivo via infections of the Greater wax moth larvae (*Galleria mellonella*). We further assessed their toxicity in the host, towards two mammalian cell lines and red blood cells. Finally, we used experimental evolution combined with whole-genome sequencing to study the potential of pathogens evolving resistance against pyoverdine treatment.

Results

Pyoverdines can inhibit the growth of human opportunistic pathogens

To assess the antibacterial properties of pyoverdines, we performed a growth-inhibition screen using a well-characterized collection of 320 natural *Pseudomonas* isolates[17,30–32]. The isolates stem from freshwater and soil communities and belong to the group of fluorescent pseudomonads (e.g, *P. fluorescens*, *P. putida*, *P. syringae*, *P. chlororaphis*) that are non-pathogenic to humans and can produce and secrete pyoverdines, a group of high iron-affinity siderophores[33].

In a first screen, we evaluated how the sterile pyoverdine-containing supernatants of the 320 isolates affect the growth of 12 human opportunistic pathogens (Table 1). We found high variation in the supernatant effect, ranging from complete pathogen growth inhibition to growth promotion compared to the mock control (Figure 1A and Figure S1A). The mean supernatant effect across all pathogens showed a bimodal distribution with two peaks at 0.47 – 0.58 (approximately 50% growth inhibition) and 1.00 – 1.10 (no growth inhibition) (Figure S1B). Our observations are consistent with previous studies, in which supernatants containing siderophores can have both growth inhibitory and stimulatory effects[21,30]. For each supernatant, we quantified the number of pathogens that experienced a

growth reduction of at least 20% compared to the mock control and found that 25 supernatants inhibited all 12 pathogens (Figure 1A and S1C).

Table 1 | Species and strains of human opportunistic pathogens used for the pyoverdine growth inhibition assay

Species and strain name	Class	Gram-staining	Frequency of inhibiting supernatants
Acinetobacter johnsonii	Gammaproteobacteria	negative	75.0
Acinetobacter junii	Gammaproteobacteria	negative	73.1
Burkholderia cenocepacia H111	Betaproteobacteria	negative	52.2
Burkholderia cenocepacia K56-2	Betaproteobacteria	negative	54.7
Cronobacter sakazakii	Gammaproteobacteria	negative	48.8
Escherichia coli K12	Gammaproteobacteria	negative	31.6
Klebsiella michiganensis	Gammaproteobacteria	negative	30.9
Pseudomonas aeruginosa PA14	Gammaproteobacteria	negative	9.7
Pseudomonas aeruginosa PAO1	Gammaproteobacteria	negative	20.9
Shigella sp.	Gammaproteobacteria	negative	57.8
Staphylococcus aureus Cowan	Bacilli	positive	47.8
Staphylococcus aureus JE2	Bacilli	positive	41.6

To confirm that the growth-inhibiting properties of the 25 most potent supernatants are indeed caused by pyoverdines and not by other agents in the supernatant, we repeated the above assay, but this time supplemented the supernatant with 40 µM $FeCl_3$. Under such iron-replete conditions, pyoverdines should not be able to substantially sequester environmental iron, and pathogen growth should therefore be restored. We identified seven top candidate supernatants for which a relative growth recovery of at least 0.2 occurred for all 12 pathogens

(Figure 1B). Among the remaining 18 supernatants, the overall rate of growth recovery was also high, indicating that pyoverdines are responsible for pathogen growth inhibition under iron-limited conditions in most cases.

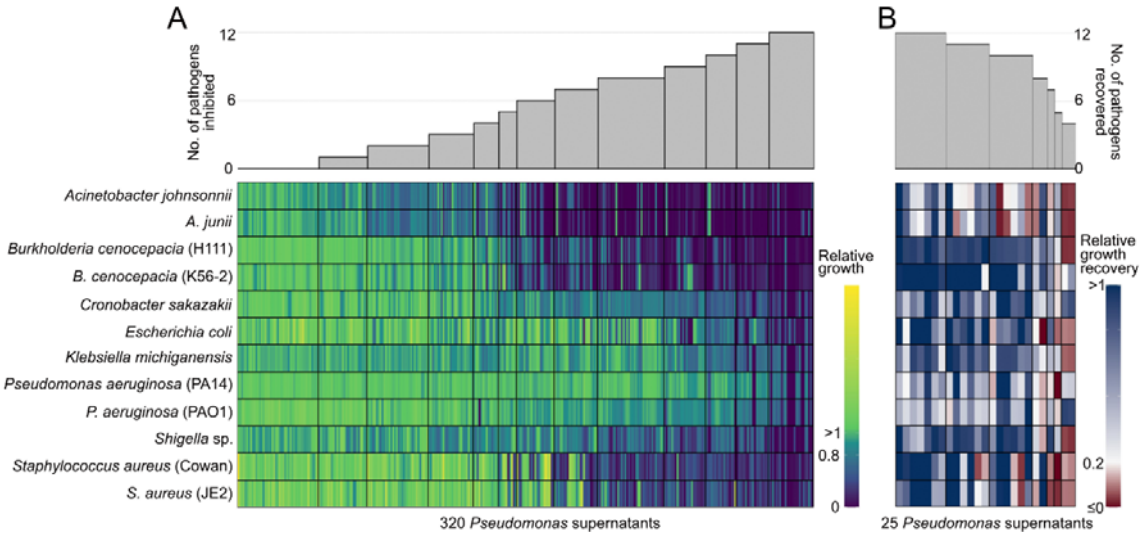

Figure 1 | Effect of supernatants from environmental *Pseudomonas* isolates on the growth of 12 human opportunistic pathogens. (A) Screen to assess the extent to which pyoverdine-containing supernatants from 320 natural *Pseudomonas* isolates inhibit the growth of 12 human opportunistic pathogens. The heatmap depicts relative pathogen growth in the supernatant treatment relative to the mock control, with values ranging from stimulation (yellow) to inhibition (blue) based on four independent replicates. Grey bars above the heatmap show the number of pathogens that were at least 20% inhibited in their growth by a given supernatant. The screen returned 25 supernatant candidates that inhibited the growth of all pathogens. (B) Control screen with the 25 supernatant candidates to check whether pyoverdine causes the observed growth inhibition. The heatmap depicts the level of growth recovery in the 12 pathogens when iron was added to the supernatant. Growth recovery in iron-rich medium indicates that pyoverdines are involved in growth inhibition in iron-limited medium. Grey bars above the heatmap show the number of pathogens that experienced a relative growth recovery of at least 0.2. The screen returned 7 supernatant top candidates for which growth recovery occurred for all pathogens under iron-rich conditions.

Growth-inhibiting pyoverdines show distinct chemical features

In previous studies, we developed a new method for pyoverdine structure elucidation from low-volume crude extracts using ultra-high-performance liquid chromatography

high-resolution tandem mass spectrometry (UHPLC-HR-MS/MS)[28,34]. These studies included the pyoverdines extracted from the seven top candidate supernatants and the analysis therein yielded five structurally different pyoverdines (Figure 2A). We found one novel pyoverdine type (**1**, from isolate 3A06) and four pyoverdine types already known from the literature (**2**-**5**). The pyoverdine from isolate 3G07 can occur in either a linear or cyclic conformation (**2a** and **2b**). Three isolates (s3b09, s3b10, s3b12), all originating from the same soil sample, had an identical pyoverdine type (**3**).

Here, we investigated whether the chemical properties of growth-inhibitory pyoverdines differ from pyoverdines that do not inhibit pathogen growth. To this end, we further elucidated the chemical structure of a set of six pyoverdines extracted from supernatants that inhibited none of the 12 pathogens, and one additional pyoverdine inhibiting the growth of 10 pathogens[28]. We found that inhibitory pyoverdines had significantly larger collision-cross sections (CCS in $Å^2$) than non-inhibitory ones ($F_{1,22}$ = 10.63, p = 0.0036, measured by ion mobility spectrometry (IMS)) (Figure 2B). As CCS values correlate with the volume of a molecule, our results suggest that inhibitory pyoverdines are larger and have more complex molecule structures than non-inhibitory pyoverdines. In contrast, there was no significant difference between the two classes of pyoverdines regarding molecule polarity ($F_{1,22}$ = 2.00, p = 0.1711, assessed by the chromatographic retention time on a reverse phase column) (Figure 2C), but molecule polarity was significantly higher for ferri- than for apo-pyoverdines ($F_{1,22}$ = 12.78, p = 0.0017). Finally, we assessed the stability of ferri-pyoverdines to derive a proxy for iron affinity. We first measured the propensity of ferri-pyoverdines to undergo collision-induced unfolding (CIU) by IMS measurements at different Δ6 voltages and found that inhibitory pyoverdines are

significantly more stable than non-inhibitory pyoverdines ($F_{1,11}$ = 7.55, p = 0.019) (Figure 2D). The same trend was observed for our second measure of stability (CE50, normalised collision energy necessary to fragment 50% of ferri-pyoverdines), but in this case, the difference between the two pyoverdine classes was not significant ($F_{1,11}$ = 1.87, p = 0.198) (Figure 2E). Taken together, the chemical analyses suggest that inhibitory pyoverdines are larger and have a higher affinity for iron than non-inhibitory pyoverdines.

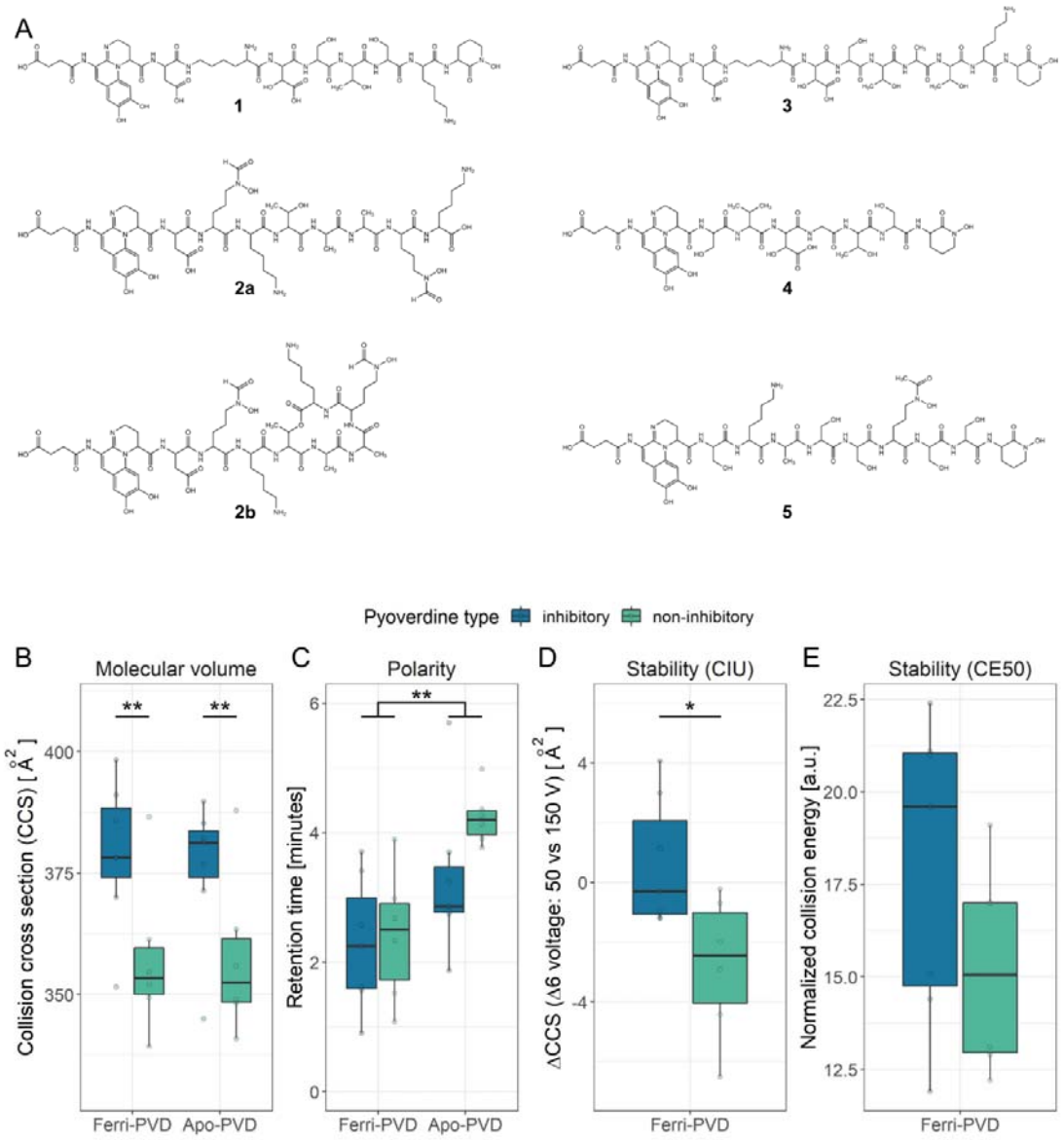

Figure 2 | Chemical structure of growth-inhibitory pyoverdines and their properties compared to non-inhibitory pyoverdines. (A) The chemical structures of the seven top candidate pyoverdines were elucidated using UHPLC-HR-MS/MS and revealed 5 unique pyoverdine structures (**1**-**5**) differing in their peptide backbone (see[28] for an in-depth chemical analysis). Pyoverdine **1** is a novel structure (from isolate 3A06). Pyoverdine **2** can occur in either a linear **2a** or a cyclic **2b** form (from isolate 3G07). Pyoverdine **3** was found in three different isolates, originating from the same soil sample (from isolates s3b09, s3b10 and s3b12). Pyoverdine **4** and **5** are from isolate s3c13 and s3e20, respectively. (B) The CCS values of inhibitory pyoverdines are higher than for non-inhibitory pyoverdines. (C) Molecule polarity, measured as the chromatographic retention time, is higher for ferri-pyoverdines (iron loaded) than for apo-pyoverdines (iron free). (D) Iron complex stability, assessed by the collision induced unfolding of ferri-pyoverdines, was significantly higher for inhibitory than non-inhibitory pyoverdines. (E) The normalised collision energy (CE50) necessary to fragment 50% of ferri-pyoverdines was not different between inhibitory and non-inhibitory pyoverdines. Box plots show the median and the first and third quartiles across the 7 inhibitory and 6 non-inhibitory pyoverdines. Whiskers represent the 1.5x interquartile range.

Pyoverdines inhibit human pathogens in a concentration-dependent manner

We purified three out of the five most potent pyoverdines and tested their efficacy against the four human pathogens *A. baumannii*, *K. pneumoniae, P. aeruginosa* and *S. aureus*. For these experiments, we decided to include the most common (s3b09), the novel (3A06), and the cyclical-linear (3G07) pyoverdines. We crude-purified all three pyoverdines using established protocols[17,35] and further purified the most common pyoverdine (s3b09) using preparative and analytical HPLC. During HPLC purification, we observed that ferribactin (the final pyoverdine precursor) was also highly abundant in the supernatant[36,37]. Due to its compromised iron-binding capacity, we used it as a negative control for which no activity against pathogens is expected[37]. As positive treatment control, we used the antibiotic ciprofloxacin. We subjected the four pathogens to the three pyoverdine variants, ferribactin, and

ciprofloxacin across a concentration gradient and measured their effects on pathogen growth (Figure 3, Figure S2).

For *A. baumannii* and *S. aureus,* we observed classical dose-response curves in all pyoverdine assays, characterized by a decrease in bacterial growth at low and intermediate concentrations, followed by a complete halt of bacterial growth at higher pyoverdine concentrations. There was a good qualitative match between the dose-response curves obtained with the HPLC vs. the crude-purified pyoverdines. Note that pyoverdine concentration is unknown for the crude extracts and is thus expressed as relative concentrations. In contrast, the pyoverdine concentration is absolute for the HPLC-purified version, allowing the determination of an IC50 value for pyoverdine s3b09, which is 5.037 µg/mL and 12.163 µg/mL for *A. baumannii* and *S. aureus*, respectively.

For *K. pneumoniae*, the pyoverdines were less effective in reducing pathogen growth. The dose-response curves for the pyoverdines s3b09 (HPLC and crude) and 3A06 showed similar trajectories and the model fits showed a growth reduction between 9-12%. The strongest inhibitory effects were found for pyoverdine 3G07 with an estimated 54% growth reduction. One reason why pyoverdines might be less effective against *K. pneumoniae* is that this species produces enterobactin, a siderophore that has higher iron affinity than pyoverdine[38].

For *P. aeruginosa*, we observed that all pyoverdines were growth inhibitory at intermediate concentrations. The initial inhibition converted into growth promotions at high pyoverdine concentrations in three out of four cases. The only exception was pyoverdine 3G07, which yielded consistent growth inhibitions of about 66%. One reason for these non-standard dose-response curves could be that *P. aeruginosa* possesses two receptors (FpvA and FpvB) for pyoverdine uptake[39]. It might thus

capitalize on the supplemented pyoverdines, especially at high concentrations via the up-regulation of the heterologous promiscuous FpvB receptor[40,41]. Our findings for *P. aeruginosa* are not unexpected and show that pyoverdine treatment should not be applied against this pathogen.

Taken together, we found that all pyoverdines are highly potent against *A. baumannii* and *S. aureus,* and one pyoverdine (3G07) is potent against *K. pneumoniae*. Especially in the case of *A. baumannii* and *S. aureus,* the pyoverdine dose-response curves follow the standard trajectory observed for antibiotics (Figure S2 for ciprofloxacin). In support of our hypothesis that the inhibitory effects of pyoverdines operate via withholding iron from pathogens, we found no growth inhibition when the pathogens were exposed to purified ferribactin (Figure S2), the non-iron chelating precursor of pyoverdine.

To further validate that the antibacterial effect of pyoverdine is due to iron sequestration, we saturated pyoverdine s3b09 with varying concentrations of iron and repeated the dose-response experiment with *A. baumannii* (Figure S3). Here, we expect pyoverdine potency to decrease because iron is no longer a growth limiting factor. Indeed, we observed that the inhibition of *A. baumannii* was greatly reduced with intermediate levels of iron supplementation (40 µm) and completely stalled with high levels of iron supplementation (200 µM) (Figure S3).

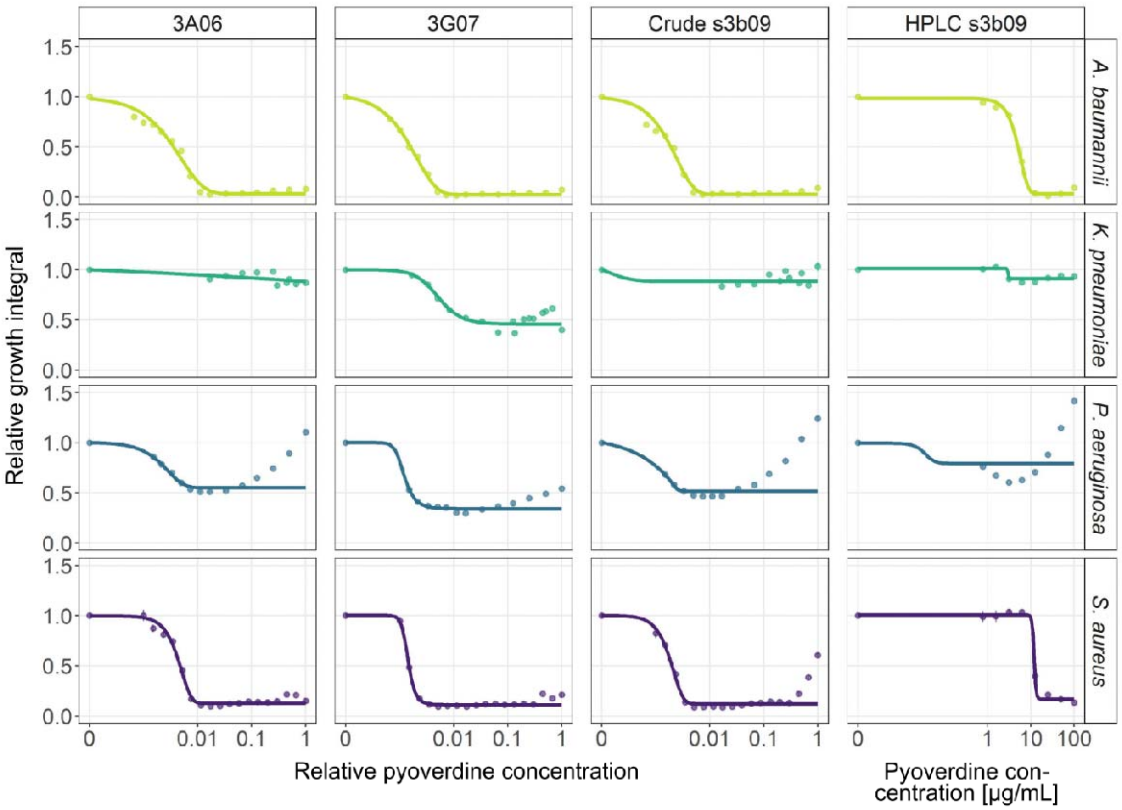

Figure 3 | Pyoverdine dose-response curves for *A. baumannii*, *K. pneumoniae*, *P. aeruginosa* and *S. aureus*. We exposed the four human opportunistic pathogens to three pyoverdines (3A06, 3G07, s3b09) that were among the most potent ones. We used crude-purified extracts of all three pyoverdines and a HPLC-purified variant for pyoverdine s3b09. The absolute concentrations of the crude-purified extracts are unknown and therefore expressed relative to the weighed amount of 6 mg. The absolute concentration of the HPLC-purified variant is given in µg/mL. Growth values are scaled relative to the untreated control in CAA medium. Dots and error bars show mean values and standard errors, respectively, across a minimum of three replicates per concentration. Dose-response curves were fitted using 4- or 5-parameter logistic regressions.

Pyoverdines have low toxicity for mammalian cell lines, erythrocytes, and hosts

We investigated the potential toxicity of crude-purified pyoverdines against mouse neuroblastoma-spinal cord (NSC-34) hybrid cells and human embryonic kidney 293 (HEK-293) cells. NSC-34 are motor neuron-like cells, which do not divide in their

differentiated state, thus mimicking established tissue. For these cells, we observed no adverse effects on cell viability at low and intermediate pyoverdine concentrations (Figure 4A), representing the doses that strongly inhibited the pathogens (Figure 3). A moderate decrease of cell viability was only observed at the highest pyoverdine concentrations (Figure 4A). Conversely, HEK-293 cells divide rapidly and inform us on whether pyoverdines interfere with cell proliferation. We indeed noticed a more pronounced effect on cell viability already at intermediate pyoverdine concentrations (Figure 4A), which suggests that pyoverdine chelates the iron required for cell proliferation.

To assess the haemolytic activity of pyoverdines, we exposed sheep erythrocytes to a concentration gradient of the crude-purified pyoverdines. We found that haemolysis was extremely low (<1%) relative to the positive control Triton X-100 surfactant for pyoverdine concentrations up to 0.5 (Figure 4B) and remained low even for the highest concentration (haemolysis rates for pyoverdines 3A06, 3G07 and s3b09 were 2.01%, 1.89% and 5.92%, respectively). This result shows that pyoverdines are unable to retrieve iron from haemoglobin.

Finally, we injected pyoverdine into the larvae of *G. mellonella* and followed host survival over time. We selected three pyoverdine concentrations (0.01, 0.05, and 0.1), which we later used for the infection experiments, and which were minimally toxic to cell lines (coloured dots in Figure 4A). We found that pyoverdine injections did not significantly reduce host survival at low and intermediate concentrations (Figure 4C and Table S1). In contrast, we observed a tendency towards higher larval mortality levels with the highest pyoverdine concentration administered, especially for 3G07, suggesting that pyoverdines can be mildly toxic for the host at high concentrations.

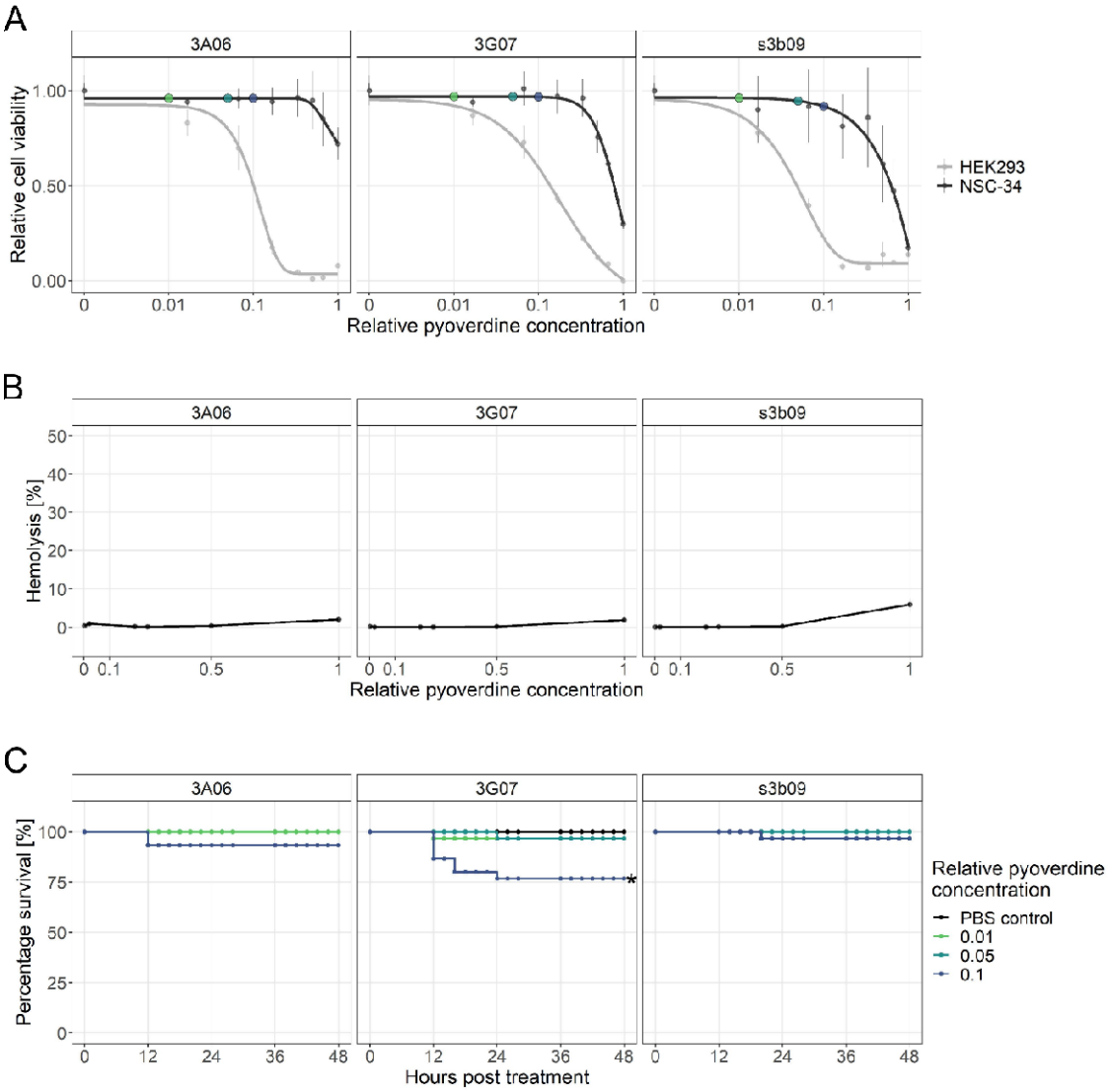

Figure 4 | Toxicity assays for pyoverdines from environmental *Pseudomonas* spp. against human cell lines, sheep erythrocytes and the host larvae of *G. mellonella*. (A) We exposed mouse neuroblastoma-spinal cord (NSC-34) and human embryonic kidney 293 (HEK-293) cells to three crude-purified pyoverdines (3A06, 3G07, s3b09) that were among the most potent ones to inhibit bacterial growth. An MTT assay was used to assess the metabolic activity of cells as an indicator of cell viability and proliferation. Cell viability data are scaled relative to the pyoverdine-free treatment, whereby dots and error bars show means and standard error across three replicates, respectively. The absolute concentrations of the crude-purified pyoverdines are unknown and concentrations are therefore expressed relative to the highest one used. Coloured dots indicate pyoverdine dosages used for the *in vivo* experiments (pyoverdines/10 µL). Dose-response curves were fitted using 5-parameter

logistic regressions. (B) We evaluated the haemolytic activity of the pyoverdines by adding them to sheep erythrocytes along a concentration gradient (range 0.002 – 1). Triton X-100 and PBS served as positive and negative control, respectively. Haemolytic activity is scaled relative to the positive control, dots and error bars show means and standard error across 6 replicates from two independent experiments, respectively. (C) To assess the toxic effects of pyoverdine on the host, we injected pyoverdines (three relative concentrations, 0.01, 0.05, 0.1) into larvae 4 hours after a mock infection with PBS. The percentage of larval survival was tracked over 48 hours post-treatment. Data stem from three independent experiments with each 10 larvae per infection and treatment.

Pyoverdine treatment increases the survival of infected hosts

We then investigated whether pyoverdines can be used to treat infections in *G. mellonella*. We used *A. baumannii*, *K. pneumoniae,* and *P. aeruginosa* as pathogens. We did not include *S. aureus* for these experiments as it is literally avirulent for *G. mellonella* given the infection loads and time frames used[42]. We first determined the bacterial infection load needed to reduce larval survival by at least 50% (Figure S4) over 48 hours. We found this to be the case with $1.8*10^5$ CFU/larvae of *A. baumannii* and $8.9*10^5$ CFU/larvae of *K. pneumoniae*. For *P. aeruginosa*, all larvae died within 48 hours even with the lowest infection dose and we decided to use 56 CFU/larvae. We infected the larvae with one of the three pathogens, and subsequently treated them with either pyoverdine (relative concentrations 0.01, 0.05 and 0.1) or a PBS control four hours post infection, followed by monitoring larval survival over time (Figure 5).

We found that the two pyoverdines 3A06 and 3G07 were effective treatments against *A. baumannii* and *K. pneumoniae* and significantly decreased the risk of death compared to untreated infections (Figure 5, Table S2). Specifically, *A. baumannii* treated with 3A06 at a concentration of 0.05 and 3G07 at a concentration of 0.01 reduced the risk of death (hazard) by 57.9% ($z = -1.973$, $P = 0.0485$) and

59.4% (z = -2.057, p = 0.0397), respectively. For s3b09, the same tendency was observed (z = -1.496, p = 0.135) albeit not significant. For *K. pneumoniae*, the pyoverdine treatments 3A06 and 3G07 (concentration of 0.01) reduced the risk of death by 51.5% (z = -2.027, p = 0.0426) and 57.6% (z = -2.341, p = 0.0192), respectively. Lower doses of pyoverdine seemed to be more effective than the highest concentration, reinforcing our observation that pyoverdine can exhibit some toxicity at higher concentrations (Figure 4C). Infections with *P. aeruginosa* led to near 100% larval mortality regardless of pyoverdine treatment and dosage so that no significant treatment effect arose. Altogether, our infection experiments show that pyoverdines are effective against the moderately virulent pathogens *A. baumannii* and *K. pneumoniae*, while they are ineffective against the fast-killing highly virulent *P. aeruginosa*.

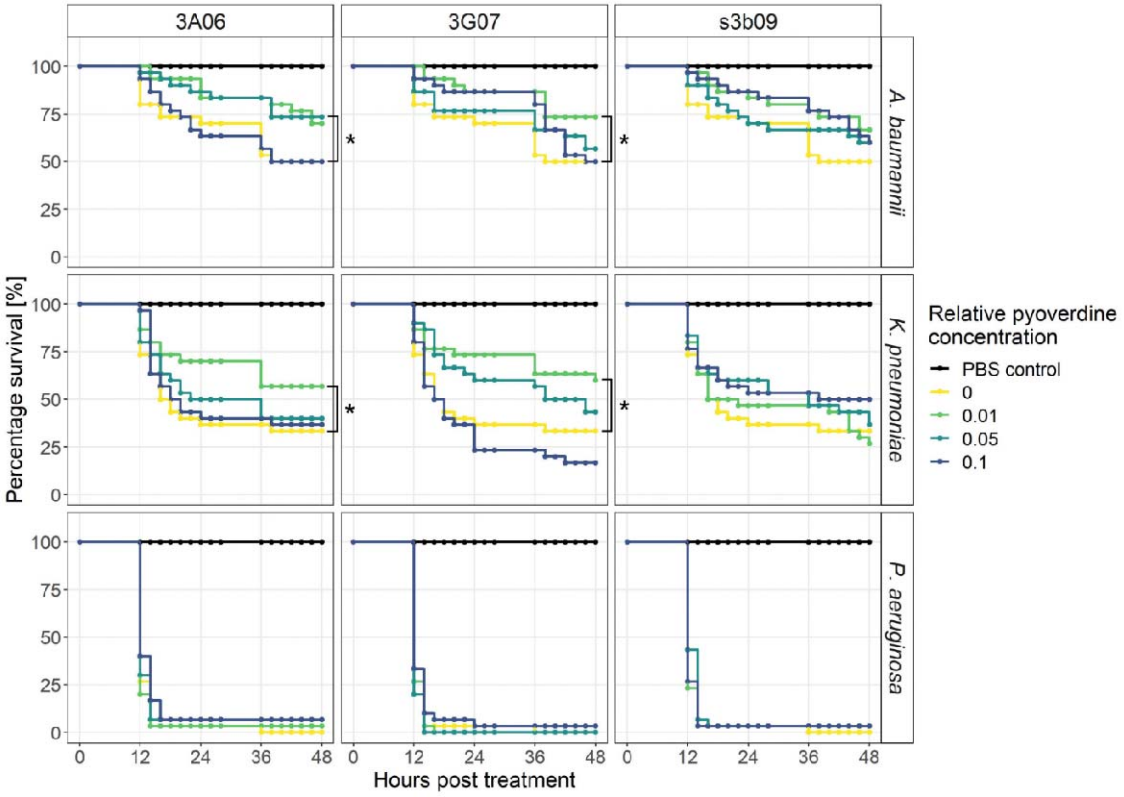

Figure 5 | Pyoverdine treatments significantly increase survival of the host *G. mellonella* when infected with *A. baumannii* and *K. pneumoniae*. Larvae of the greater

wax moth were first infected with either *A. baumannii*, *K. pneumoniae*, or *P. aeruginosa* and then treated with one of three pyoverdines (3A06, 3G07, or s3b09) at four relative pyoverdine concentrations (0, 0.01, 0.05, 0.1). All panels show the larvae survival over 48 hours post-treatment. Data stem from three independent experiments with each 10 larvae per infection and treatment. Asterisks indicate significant differences in larval survival between treated and untreated infections based on Cox proportional hazard regressions ($p < 0.05$).

Pathogens show low levels of resistance evolution against pyoverdine treatment

We assessed the ability of *A. baumannii*, *K. pneumoniae*, *P. aeruginosa* and *S. aureus* to evolve resistance against the pyoverdine treatment by exposing all pathogens to both single pyoverdine treatments (3A06, 3G07, and s3b09) and combination treatments (double and triple combinations) over 16 days of experimental evolution. One exception was *K. pneumoniae*, which was only exposed to 3G07 as only this pyoverdine was inhibitory. We had six independent lineages (populations) per pathogen and treatment combination (see Table S2 for treatment concentrations). We further subjected all pathogens to the antibiotic ciprofloxacin as positive control in which resistance evolution is expected. Additionally, we let the pathogens grow in untreated medium to control for medium adaptation. Overall, we had 180 lineages that were transferred daily to fresh medium.

After experimental evolution, we observed that all four pathogens grew significantly better under ciprofloxacin treatment than the ancestor and beyond the level observed for medium adaptation (Table S3; Figure 6A). This provides strong evidence for pervasive resistance evolution against this conventional antibiotic. In contrast, we found that none of the four pathogens treated with pyoverdines experienced a significant increase in growth relative to the observed level of medium

adaptation (Table S3, Figure 6A), suggesting low potentials of resistance evolution at the population level.

However, population screens can hide the presence of resistant clones within populations. We thus picked eight random clones from two populations for each of the pyoverdine single treatments and one combo treatment for each pathogen. With a total of 208 clones, we repeated the above growth assay and expressed clonal growth as fold-change relative to the growth of populations evolved in medium alone (Figure 6B). For *A. baumannii* and *K. pneumoniae*, the average growth fold-change across clones was 1.02 ± 0.004 and 0.84 ± 0.02, respectively, and there was no sign of resistant clones being present in populations. This was different for *P. aeruginosa* and *S. aureus*, for which we observed high variation in growth fold-changes across clones, with many clones growing moderately better than the medium controls. The growth increase across clones was 1.11 ± 0.02 and 1.10 ± 0.02, and significant in three and two population of *P. aeruginosa* and *S. aureus*, respectively. Thus, the clonal screen indicates some level of adaptation to pyoverdine treatment for these two pathogens.

To obtain insights into the genetic basis of putative resistance evolution, we sequenced the whole genomes of 52 evolved clones (16 per pathogen, except 4 for *K. pneumoniae*), 16 medium-evolved control populations and the 4 ancestors. We first mapped reads to the reference genomes and then to our ancestors. We called single nucleotide polymorphisms and small deletions/insertions that arose during experimental evolution (Figure 6B). We observed that growth peaks in clones with one mutation and decreases in clones with more mutations (Figure 6C, linear fit: $F_{1,66} = 7.51$, $p = 0.0079$), a pattern that suggests positive selection of a few specific advantageous mutations. Next, we filtered out mutations in genes that occurred at

least twice in the control populations and identified 14 (*A. baumannii*), 0 (*K. pneumoniae*), 15 (*P. aeruginosa*), and 18 (*S. aureus*) mutations that exclusively arose under pyoverdine treatment and could thus be associated with resistance evolution. We classified the mutated genes in functional categories (Figure 6D, Table S4) and found that genes relevant for biofilm and motility formed the only category in which mutations were both frequent and consistently associated with increased growth in *P. aeruginosa* and *S. aureus* (Figure 6D).

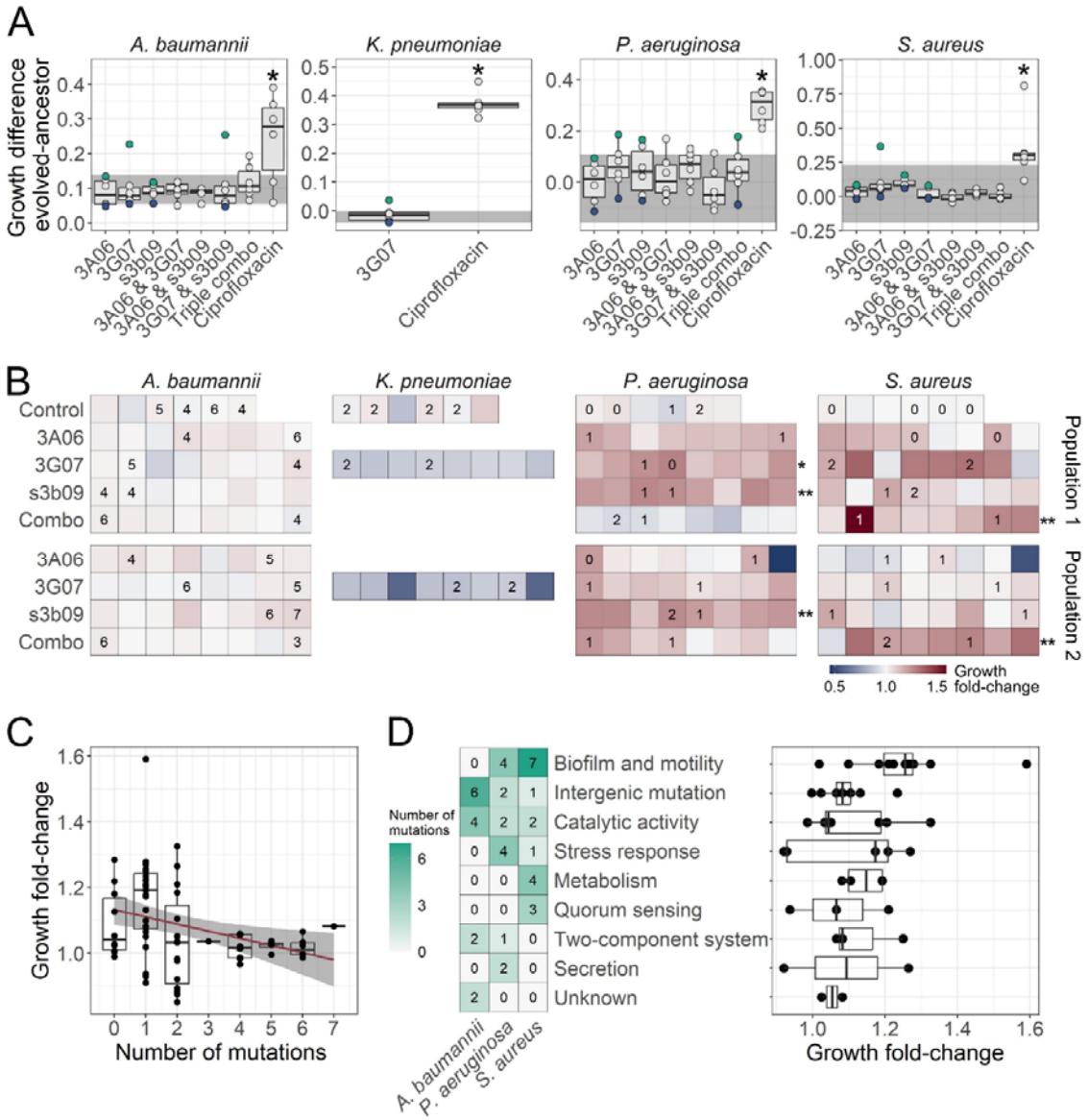

Figure 6 | Phenotypic and genotypic analysis of experimentally evolved pathogens reveal weak levels of resistance evolution against pyoverdine treatment. (A) We exposed evolved and ancestral pathogen populations to the treatment in which they evolved in and quantified their growth (area under the curve). Growth values were scaled relative to the ancestor in untreated medium, and the panels show the scaled growth differences between evolved and ancestral populations. The shaded areas show the scaled growth difference between the ancestor and the populations evolved in untreated medium and is representative of medium adaptation. The blue and green dots represent the pathogen populations with the lowest (population 1) and highest (population 2) scaled growth difference, respectively, which were subsequently used to pick clones. The dots show mean values across two independent replicates and asterisks show significant growth increases relative to the medium-adapted control. Box plots show the median and the first and third quartiles across the 6 independently evolved populations. Whiskers represent the 1.5x interquartile range. (B) We repeated the above growth assays with 208 individual clones evolved under pyoverdine treatment and 24 populations evolved in medium alone (control). Each square represents a clone or a control population, and the number indicates the number of mutations identified based on whole-genome sequencing. The heatmap shows the fold-change in growth relative to the evolved control populations. Asterisks depict significant fold-increases in growth compared to control populations. (C) Relationship between the number of mutations and fold-change in growth across all sequenced clones and populations (n = 68). (D) Heatmap showing the number of mutations per pathogen and per functional gene categories across clones together with the respective fold-change in growth (n = 47).

Discussion

We investigated whether pyoverdines produced by environmental *Pseudomonas* spp. have antibacterial activities against human opportunistic pathogens through iron sequestration and withholding this trace element from pathogens. Our screen involving 320 environmental isolates and 12 pathogen strains revealed five top pyoverdine candidates with broad-spectrum activity. These candidates could be distinguished from non-inhibitory pyoverdines by their high CCS values (standing for larger and more complex molecules) and their higher iron complexation stability.

Experiments with crude- and HPLC-purified pyoverdines showed that pyoverdines completely stall the growth of *A. baumannii* and *S. aureus*, while showing intermediate activity against *K. pneumoniae* and *P. aeruginosa*. When administered as treatment to infected *G. mellonella* larvae, we observed significantly increased host survival rates in infections with *A. baumannii* and *K. pneumoniae*, demonstrating that pyoverdine exhibits antibacterial activity in hosts. Furthermore, we found low toxicity of pyoverdines at effective concentrations and observed low potentials for resistance evolution. Overall, our results reveal pyoverdines from non-pathogenic *Pseudomonas* spp. as potent antibacterials against several human opportunistic pathogens.

Our novel treatment approach assumes that pyoverdines sequester iron and thereby induce iron starvation and growth arrest in pathogens. Several of our findings support this view. First, the growth-inhibiting effect of our top pyoverdine candidates exclusively occurred under iron-limited conditions, while pathogen growth was restored under iron-replete conditions (Figure 1, Figure S3). Second, non-inhibitory ferri-pyoverdines were more prone towards collision induced unfolding than inhibitory ferric-pyoverdines (Figure 2D), suggesting that inhibitory pyoverdines have a higher iron binding affinity. Third, the pyoverdine precursor ferribactin did not inhibit pathogen growth (Figure S2). The two molecules are identical apart from one ring in the chromophore core that is not cyclized and not oxidized in ferribactin, which compromises the binding of iron. These findings suggest that pyoverdine does not target the pathogens directly, but rather indirectly via the induction of iron starvation.

We observed that pyoverdines showed pathogen-specific efficacies in curbing bacterial growth (Figure 3). We propose that differences can be explained by the various strategies of these pathogens to cope with iron stress. *A. baumannii* and *S.*

468 *aureus* produce siderophores that have a much simpler chemical structures than
469 pyoverdines and are expected to bind iron with lower affinity (*A. baumannii*:
470 acinetobactin (association constant: 10^{26} M^{-1}), fimsbactin (10^{27} M^{-1}) and
471 baumannoferrin (unknown)[43–45], *S. aureus*: staphyloferrin A+B (unknown)[46]) than
472 pyoverdine (10^{32} M^{-1})[29]. Hence, the growth suppression of *A. baumannii* and *S.*
473 *aureus* most likely occurs because their siderophores are too weak to successfully
474 compete with pyoverdine. The situation is different for *K. pneumoniae*, which
475 produces enterobactin, the siderophore with the highest known iron affinity (10^{52} M^{-}
476 ^{1})[38]. Consistent with the concept of iron competition, we observed that pyoverdine
477 treatment is less effective against *K. pneumoniae*, and was only potent for one out of
478 three pyoverdines (3G07, Figure. 3). Finally, pyoverdine treatment is not expected to
479 work well against *P. aeruginosa*, which itself produces a version of this siderophore.
480 The two competing pyoverdines likely have similar iron affinities and the presence of
481 pyoverdine receptors in the pathogen might foster the uptake of the supplemented
482 pyoverdine. Our results indeed support the view that pyoverdine treatment is not
483 effective against *P. aeruginosa*. Taken together, we predict that pyoverdine treatment
484 could be highly potent against certain pathogens like *A. baumannii* and *S. aureus*
485 that have less efficient siderophores and are unable to use the pyoverdine as iron
486 source.

487 Not only bacteria but also host cells need iron. Consequently, pyoverdine
488 treatment could negatively affect host iron homeostasis. Our toxicity assays reveal
489 that there is a range of pyoverdine concentrations for which only mild adverse effects
490 against cell lines and *G. mellonella* larvae are observed and no haemolysis occurs.
491 Especially the finding that pyoverdines have no negative effects on the survival of
492 non-replicating NSC-34 cells is encouraging, as this cell line is representative of

intact host tissue, in which iron is bound to strong chelators such as transferrin, lactoferrin or ferritin[47,48]. The result that pyoverdines are unable to obtain iron from haemoglobin is encouraging, too. Previous work showed that the pyoverdine of *P. aeruginosa* can retrieve iron from human transferrin when working in concert with proteases (proteolytically degrading transferrin)[49] or phenazines (spontaneously reducing ferric to ferrous iron)[50]. However, these *P. aeruginosa* specific mechanisms require the presence of this pathogen[51], which is not the case when purified pyoverdines are used as a treatment against other pathogens like *A. baumannii*. Nonetheless, we found that pyoverdines can have certain adverse effects, especially for the rapidly proliferating HEK293 cells (Figure 4). These cells represent a regenerating tissue and thus have high iron demands. Similarly, we observed mild adverse effects for some pyoverdines (3G07) when administered at high concentrations to *G. mellonella* larvae (Figure 5). These findings corroborate the results from previous studies on *Caenorhabditis elegans*, where pyoverdines were found to interfere with host iron homeostasis[52,53]. These considerations highlight that finding the right pyoverdine concentration will be key to meet the fine line between maximizing pathogen inhibition and minimizing tissue damage. By contrast, the adverse host effects of pyoverdines might come with additional opportunities, for instance in cancer therapy, where siderophores reduce iron levels in tumours and slow tumour progression[54].

We propose that pyoverdine treatment could synergistically interact with the host innate immune system. Mammalian neutrophils produce siderocalin to sequester bacterial siderophore-iron complexes, rendering them non-functional[47]. While this strategy is efficient against many siderophores, some bacteria have evolved so-called stealth siderophores that no longer bind to siderocalin.

Pyoverdines are such stealth siderophores[55]. Regarding pyoverdine treatment, this means that pathogens with regular siderophores will hit a double wall: their siderophores are immobilized by siderocalins, while pyoverdines lock away the remaining iron.

Another promising finding of our work is that the potential for resistance evolution against pyoverdines seems low. Conceptually, one reason for low resistance evolution could be that pyoverdines, unlike many antibiotics, are not internalized into bacterial cells. Thus, classic resistance mechanisms such as reduced drug influx, increased drug efflux, and intra-cellular target modification cannot operate[56]. We initially expected that resistance evolution would involve mechanisms that improve the pathogen's iron acquisition. This could include the up-regulation of the pathogen's own siderophores or switching from siderophore-based ferric iron acquisition to the use of reductases that foster ferrous iron uptake[56]. However, our sequencing analysis did not reveal mutations in genes associated with iron uptake systems. One explanation is that such mutations (albeit beneficial) might not reach high frequencies in populations because increased siderophore production and secretion would increase the iron acquisition of resistant and non-resistant cells alike[56]. We instead observed an overrepresentation of mutations in biofilm and motility genes in *P. aeruginosa* and *S. aureus*. While we do not know the phenotypes of these mutations, one possibility is that increased biofilm formation could offer some protection against pyoverdine treatment, for example by restricting pyoverdine from chelating free iron. Important to note is also that patterns of resistance evolution may differ between *in vitro* and *in vivo* settings[4,57]. For example, our experimental evolution setup did not allow for horizontal transfer of siderophore receptors, a

scenario that might occur in the context of polymicrobial infections and confer resistance to pyoverdine therapy.

In conclusion, our treatment approach using pyoverdine is based on the principle of paying like with like. Pathogens secrete siderophores to scavenge iron for their growth. We add a strong heterologous siderophore as treatment to withhold iron from pathogens to curb their growth. The idea to target bacterial iron up-take mechanisms has been highlighted in the literature for quite some time[13,58–61]. While certain approaches focussed on the inhibition of siderophore synthesis[58], others were based on the administration of synthetic iron chelators[13]. However, synthetic iron chelators are often toxic and have lower iron affinities compared to bacterial siderophores. The advantage of our approach is that we capitalize on naturally evolved iron chelators from non-pathogenic species with extremely high iron affinity. We have shown that these natural iron chelators have a high potency to make iron inaccessible to pathogens, while showing low toxicity for hosts at treatment effective concentrations and low potentials for resistance evolution. They could become a new source of efficient antibacterials either as independent treatment or in combination with conventional antibiotics.

Material and methods

Bacterial strains

We used a strain collection of 320 natural isolates, originating from soil and pond habitats. The isolates originate from 16 independent soil and water samples (20 isolates per sample) collected on the Campus Irchel Park of the University of Zurich. In previous work, we have extensively studied and characterized all isolates[17,30–32]. Particularly, sequencing of the *rpoD* housekeeping gene confirmed that 315 isolates

belong to the group of fluorescent pseudomonads that are non-pathogenic to humans. For the remaining five isolates, the *rpoD* gene could not be amplified, yet they were still included in our study. Moreover, siderophore screens previously revealed that a large proportion of the isolates can produce and secrete pyoverdines, the high-iron affinity siderophores we focus on in our study. The exact sampling and isolation procedures together with the pyoverdine production profiles are described elsewhere. All bacterial natural isolates and pathogenic species used in our study will be available from the authors upon request.

We used a collection of 14 strains of opportunistic human pathogens (Table 1). Twelve of these strains were used for the pyoverdine growth inhibition screen: *A. johnsonii*, *A. junii*, *C. sakazakii*, *K. michiganensis* (belonging to the *K. oxytoca* complex)[62] and *Shigella* sp. (kindly provided by the laboratory of Leo Eberl, University of Zurich), and *B. cenocepacia* strains H111 and K56-2, *P. aeruginosa* strains PA14 and PAO1, *E. coli* K12 and *S. aureus* strains Cowan and JE2 from our own strain collection. *A. baumannii* (DSM 30007) and *K. pneumoniae* (DSM 30104) were purchased from the German Collection of Microorganisms and Cell Cultures GmbH

Culturing conditions

Pathogen overnight cultures were grown in either 8 mL tryptic soy broth (TSB; for the two *S. aureus* strains) or 8 mL lysogeny broth (LB; all other pathogens) in 50 mL tubes at 37 °C and 220 rpm agitation. Following two washing steps with 0.8% NaCl, we adjusted the overnight cultures to an optical density at 600 nm (OD_{600}) of 1. For overnights of environmental isolates, we followed the same procedure when working with low sample sizes, with the only difference being that culturing occurred at 28 °C.

For the large-scale screening experiments, we grew environmental isolates in 200 µL LB in 96-well plates shaken at 170 rpm. Cultures from plates were then directly used for experiments.

For all main experiments (screen for bioactive pyoverdines and dose-response curves), we used casamino acid (CAA) medium (1% casamino acids, 5 mM K_2HPO_4 * $3H_2O$,1 mM $MgSO_4$*7 H_2O, 25 mM HEPES buffer). This medium contains low levels of iron, triggering pyoverdine production[63].

Supernatant screening assays

In a first step, we created sterile supernatants from all the 320 *Pseudomonas* isolates. To do so, we transferred 2 µL of overnight cultures (grown in 96-well plates in LB in four-fold replication for 24 hours as described above) to new plates containing 200 µL of CAA medium supplemented with 250 µM 2,2'-bipyridyl. Cultures were incubated for 24 hours and subsequently centrifuged at 2250*g* for 10 minutes. The supernatants were transferred to 0.2 µm membrane filter plates (PALL AcroPrep Advance), centrifuged a second time, and frozen at -20 °C.

For the supernatant screening assay, the pathogens were cultured and diluted as described above and added to 140 µL CAA medium in 96-well plates. We added 60 µL of thawed *Pseudomonas* supernatants (30%) or 0.8% NaCl as control and incubated the plates at 37 °C and 170 rpm. Growth was measured as OD_{600} after 24 hours using a Tecan Infinite M-200 plate reader (Tecan Group, Männedorf, Switzerland). We then scaled the growth of pathogens in the supernatant relative to their growth in the control treatment. Relative growth values smaller and larger than one indicate growth inhibition and promotion by the supernatant, respectively.

To test whether pyoverdine is responsible for pathogen growth reduction, we repeated the screening assay but supplemented the CAA medium containing the *Pseudomonas* supernatants with 40 µM $FeCl_3$. In this iron-rich condition, pyoverdine should not be able to limit iron availability and thus pathogen growth should be restored. In contrast, if pathogen growth is still inhibited upon iron supplementation, other components in the supernatant than pyoverdine should be responsible for growth inhibition.

Structure elucidation of pyoverdine and analyses of chemical properties

From the seven top supernatant candidates that inhibited all twelve pathogens, we extracted the pyoverdines and elucidated their structure. For this purpose, we have developed a new protocol that allows structure elucidation from low volume supernatants using UHPLC-HR-MS/MS. The methodological details are described in Rehm *et al.*[28].

Afterwards, we assessed whether growth inhibiting pyoverdines can be distinguished from non-inhibiting pyoverdines by their chemical properties. We focussed on polarity, CCS values, and stability upon collision induced unfolding or fragmentation. Detailed protocols and instrument settings can be found in [28,34]. We first purified the pyoverdines from the supernatants using solid-phase extraction. Next, we ran the samples through an HSS C18 column of the Vanquish UHPLC system (Thermo Fisher Scientific, Waltham, MA, USA) using formic acid (0.1%) as an eluent additive and MeCN as the organic phase and recorded the retention times (as a measure for polarity). We also measured the CCS values of pyoverdines and ferri-pyoverdines on a trapped ion mobility spectrometry (TIMS)-TOF-MS instrument (timsTOF Pro™, Bruker, Bremen, Germany) at a $\Delta 6$ voltage of 100 V. Finally, we

assessed the stability of ferri-pyoverdines with two approaches. First, we investigated the proneness of ferri-pyoverdines to undergo collision induced unfolding (CIU). For this, we determined the difference in CCS values of the ferri-pyoverdines (ΔCCS) at a Δ6 voltage of 50 V (no structural unfolding is stimulated) and of 150 V (structural unfolding takes place depending on the stability of the iron complex). Second, we measured the normalised collision energy necessary to fragment 50% of ferri-pyoverdine ions (CE50). This experiment was conducted on a Q Exactive hybrid quadrupole-Orbitrap mass spectrometer (Thermo Fisher Scientific, Waltham, MA, USA). Ferri-pyoverdine ions were isolated and fragmented at increasing normalised collision energies (NCE) using parallel reaction monitoring (PRM), while the ion intensity of the intact ion precursor was evaluated.

Crude pyoverdine purification

To test the efficacy of the pyoverdines against the four focal human opportunistic pathogens (*A. baumannii*, *K. pneumoniae*, *P. aeruginosa* (PAO1), and *S. aureus* (JE2)), and to assess their cytotoxicity against human cell lines, we crude-purified three pyoverdines (3A06, 3G07, s3b09). The three pyoverdines were among the five most potent ones identified in our supernatant screening assay. We adapted the method for pyoverdine purification from previous studies[17,35]. Briefly, 500 mL CAA medium was supplemented with 250 µM of the synthetic iron chelator 2,2'-bipyridyl to create an iron-limited environment and inoculated with 2 mL of washed overnight *Pseudomonas* cultures. We incubated the cultures at 28 °C for 120 hours with agitation (170 rpm). Cultures were then centrifuged at 15,049*g* for 15 minutes. We then harvested the supernatant and adjusted its pH to 6 using 1 M HCl. We ran the supernatants over Amberlite XAD-16N resin (Sigma Aldrich, Switzerland) columns at a rate of 2 drops per second and cleared the column of any salts by using 500 mL

Milli-Q water. Pyoverdines were then eluted with 50% methanol and fractions of 50 mL were collected. Fractions containing the highest amount of pyoverdine (measured by fluorescence, excitation: 400 nm and emission: 460 nm), were pooled. After evaporation of the methanol, we lyophilized the samples for 24 hours and stored them at -20 °C. As the crude purified extracts may contain small impurities, the exact pyoverdine concentration is unknown and the concentrations. For the figures, concentrations were divided by 6 mg/mL (highest concentration used) and expressed as relative concentrations.

HPLC purification of pyoverdine and ferribactin

To further validate that pyoverdines are the compounds that induce pathogen growth inhibition, we purified the most common pyoverdine (s3b09) among the most potent pyoverdines from our screens using reversed-phase high-performance liquid chromatography (HPLC). For this, we first crudely purified the pyoverdine from 9 L supernatant as described above. The crude extract was then dissolved in water and fractionated by preparative HPLC at room temperature (Agilent 1260 Infinity system, equipped with a Phenomenex Luna 5 µm C18 21.2 x 250 mm column). Ultraviolet (UV) detection was carried out at λ = 210 nm, 230 nm, 280 nm, 350 nm, 400 nm, and 460 nm. Deionized water (Milli-Q, Millipore) (solvent A) and acetonitrile (solvent B) were used as the mobile phase with a flow rate of 15 mL/minute. We eluted with a gradient of 5% – 100% solvent B in 40 minutes, followed by isocratic conditions at 100% solvent B for 10 minutes. The fractions containing pyoverdine were identified based on the HR-ESI-MS data acquired on a Thermo Scientific Q Exactive hybrid quadrupole-orbitrap mass spectrometer (scan range 100–2500 *m/z*, capillary voltage 4500 V, dry temperature 200 °C) coupled to an UltiMate 3000 UHPLC system

(Dionex, equipped with a Kinetex 2.6 µm XB-C18 150 x 4.6 mm column; solvent A: deionized water; solvent B: acetonitrile; gradient, 5% B for 30 seconds increasing to 100% B in 15.5 minutes and then maintaining 100% B for 5 minutes; flow rate 0.6 mL/minute; UV–Vis detection 200–600 nm). The fractions containing pyoverdine eluting at a retention time (RT) of 3.84 minutes in the LC-MS chromatogram (Figure S5) were further purified on a semi-preparative reverse phase HPLC at room temperature (Agilent 1260 Infinity system, equipped with a Phenomenex Luna 5 µm Phenyl-Hexyl 10 x 250 mm column, λ = 210 nm, 230 nm, 280 nm, 350 nm, 400 nm, and 460 nm monitored by UV detection). The elution gradient was increased from 5% to 15% solvent B for 30 minutes followed by a gradient shift from 15% - 100% in 5 minutes, and finally isocratic condition at 100% solvent B for 5 minutes. During the pyoverdine purification we noted high amounts of the precursor molecule ferribactin (RT of 2.42 minutes in the LC-MS chromatogram; Figure S6). We thus purified it alongside with pyoverdine using the same method.

Dose-response curves

To determine the inhibition potential of crude- and HPLC-purified pyoverdines, as well as ferribactin, we subjected *A. baumannii*. *K. pneumoniae*, *P. aeruginosa* and *S. aureus* to serially diluted extracts. For this, the extracts were dissolved in CAA medium, filter sterilized and diluted in the same medium. Bacterial overnight cultures were grown and prepared as described above and added to a total of 200 µL medium on a 96-well plate with 4 replicates per extract dilution. As positive control where growth inhibition is expected, we subjected all three pathogens to a dilution series of the antibiotic ciprofloxacin (highest concentration 4 µg/mL), in the exact same way as for the extracts. We incubated the plates at 37 °C statically in the plate reader and

717 measured the OD_{600} every 15 minutes for 24 hours. Before each measurement,
718 plates were shaken for 15 seconds. We repeated the experiment up to five times with
719 different initial extract starting concentrations. This was done to ensure that the full
720 dose response to pyoverdine was captured. Thus, sample size per individual extract
721 concentration varied between four and 20 replicates. We subtracted the blank values
722 and the background values caused by the treatment of the respective extract
723 concentration from the measured growth data and calculated the integral (area under
724 the growth curve) using the R package Growthcurver[64]. We then expressed growth
725 relative to the control medium, where bacteria grew in CAA without extract or
726 antibiotic addition. Finally, we plotted extract/antibiotic concentration vs. relative
727 growth and fitted dose-response curves (see below).
728
729 **Cytotoxicity assays**
730 To determine the cytotoxicity of pyoverdine treatments against mammalian cells, we
731 subjected human embryonic kidney 293 (HEK-293) and mouse motor neuron-like
732 neuroblastoma-spinal cord hybrid (NSC-34) cells to the crude extract of the three
733 most potent pyoverdines (3A06, 3G07, s3b09). HEK-293 cells (Invitrogen, R78007)
734 were cultured in Dulbecco's modified Eagle medium (DMEM; Sigma, D5671)
735 supplemented with 10% fetal bovine serum (FBS; Gibco, 10270-106), 1X GlutaMAX
736 (Gibco, 35050-061), 100 U/mL penicillin and 100 µg/mL streptomycin (Gibco, 15140-
737 122). NSC-34 cells (Bioconcept, CLU140) were proliferated on Matrigel (Corning,
738 354234)-coated dishes in DMEM supplemented with 10% FBS, 1X GlutaMAX, 100
739 U/mL penicillin and 100 µg/mL streptomycin. For experiments, differentiation was
740 induced by switching to DMEM/F12 medium (Gibco, 21331-020) supplemented with
741 1X GlutaMAX, 1X B27+ supplement (Gibco, 17504-044), 1X N2 supplement (Gibco,

17502-048), 20 ng/mL BDNF (PeproTech, 450-02), 20 ng/mL GDNF (PeptroTech, 450-10), 100 U/mL penicillin and 100 µg/mL streptomycin. All cells were cultured at 37 ºC with saturated humidity and an atmosphere of 5% CO_2. Then, 10,500 cells/well were plated on 96-well plates (Greiner Bio-One, 655090) and, after 48 hours, the culture medium was replaced and the pyoverdines were added at the appropriate concentrations. For this, pyoverdine stocks at 240 mg/mL were diluted in MilliQ water such that the addition of 5 µL of the pyoverdine solution to 195 µL of the culture medium resulted in final relative concentrations between 1 and 0.016. As the exact pyoverdine concentration in the crude extracts is unknown, the above concentrations were divided by the highest concentration used (6 mg/mL) and expressed as relative concentrations in the figure. After further 48 hours, the pyoverdine-containing culture medium was removed, and cells were incubated with 1 µg/mL thiazolyl blue tetrazolium bromide (Sigma, D5655) in 100 µL of fresh medium for 1.5 hours (NSC-34) or 40 minutes (HEK-293). The reaction was stopped, and formazan crystals simultaneously solubilized with the addition of 100 µl of a solution containing 10% sodium dodecyl sulfate (SDS; Sigma-Aldrich, 05030) and 0.03% HCl (Supelco, 100319). Finally, the absorbance of cell debris and other contaminants at 630 nm were subtracted from the absorbance of the solubilized formazan at 570 nm.

Haemolysis assay

To determine the haemolytic activity of pyoverdines, we quantified sheep erythrocyte haemolysis at different pyoverdine concentrations. We first centrifuged 25 mL of fresh sheep blood (Chemie Brunschwig AG, Switzerland) in a 50 mL tube at 1500*g* for 5 minutes at 4 °C. Plasma was then gently aspirated, replaced by PBS and tubes were gently inverted to mix. This washing procedure was repeated three times.

Pyoverdines were diluted in PBS to final relative concentrations of 1, 0.5, 0.25, 0.2, 0.02, and 0.002. PBS and 0.1% Triton X-100 (Sigma Aldrich, Switzerland) served as negative and positive control, respectively. 100 µL erythrocyte solution was mixed with either 100 µL pyoverdine solution or the controls in a 96-well plate in triplicates. Following an incubation at 37 °C and 120 rpm for 1 hour, the plate was centrifuged at 1036*g* for 5 minutes at 4 °C. Subsequently, 100 µL of the supernatant were transferred to a new 96-well plate. Haemoglobin release was measured at 570 nm in the plate reader and the percent haemolysis was calculated relative to the positive control (% haemolysis = (OD570 of sample – negative control) / (positive control – negative control)).

Infection model

We tested the efficacy of the pyoverdine treatment in the host model *G. mellonella*. All larvae were ordered from a local vendor (Bait Express GmbH, Basel, Switzerland) and stored without food at 16 °C in the dark for up to 3 days. In a first step, we determined the mean weight of 336 final instar *G. mellonella* larvae (mean = 435 mg). For all subsequent experiments, we weighed the larvae and only used individuals with a mean weight ± 20% (range: 340 mg - 530 mg). Larvae were immobilized on ice for 15 minutes, surface-sterilized with 70% ethanol and randomly distributed to individual wells on 24-well plates. 10 larvae were used per infection-treatment combination. To inject bacteria and to administer treatments, we used sterile needles (Sterican 26G, 0.45 x 12 mm (Braun)) and syringes (1 mL injekt-F (Braun)) attached to a syringe pump (New Era Pump Systems Inc, model NE-300) set to a flow rate of 5 mL/hour. For both infection and treatment delivery, a volume of 10 µL per larvae was injected between the posterior larval prolegs.

For infection experiments, we grew *A. baumannii*, *K. pneumoniae* and *P. aeruginosa* overnight as described above, washed them twice with PBS and diluted them to an OD_{600} of 1 in PBS. This OD_{600} corresponds to $4*10^8$ CFU/mL of *A. baumannii* and $9*10^8$ CFU/mL of *K. pneumoniae* and *P. aeruginosa*. We conducted a first experiment to determine the infection dose that kills approximately 50% of the larvae (LD_{50} value). For this, we diluted the cells in PBS and injected a range of bacterial dilutions into the larvae (in a volume of 10 µL, Figure S4). From now onwards, we express the infectious dose as CFU/larvae. For *A. baumannii*, we tested dilutions between $4*10^1$ - $4*10^6$ CFU/larvae and found that $1.8*10^5$ CFU/larvae corresponded to LD_{50}. For *K. pneumoniae*, we tested dilutions between $9*10^1$ - $9*10^6$ CFU/larvae with $8.9*10^5$ CFU/larvae being closest to LD_{50}. Finally, for *P. aeruginosa* we tested dilutions between 4 - 116 CFU/larvae and found that it was not possible to determine an LD_{50} value for this species, because all CFU/larvae doses lead to a 100% death rate (Figure S4). For the main experiments, where we treated infections with pyoverdine, we used the LD_{50} values for *A. baumannii* and *K. pneumoniae*, and 56 CFU/larvae for *P. aeruginosa*. In addition, we administered 10 µL/larvae of sterile PBS as a negative control. To allow pathogens to establish an infection, larvae were incubated at 37 °C in the dark for 4 hours.

To treat infected larvae, pyoverdines 3A06, 3G07, and s3b09 were used at three concentrations that were non-toxic for the NSC-34 cells. For this, we prepared stocks of 60 mg/mL, 30 mg/mL, and 6 mg/mL of crude pyoverdines. Since the injected treatment volume was 10 µL per larvae, the final pyoverdine concentrations were 0.6 mg, 0.3 mg, and 0.06 mg per larvae, respectively. When scaling theses concentrations to the doses used for the *in vivo* dose-response curves (Figure 4), the relative pyoverdine concentrations were 0.1, 0.05 and 0.01. Pyoverdine treatments

were administered as described above with the larvae being immobilized on ice for 15 minutes.

Following treatment, larvae were kept at 37 °C in the dark. From the 12th hour post infection (hpi), their survival was checked every other hour for a total of 48 hpi, with a break between 28 and 36 hpi. To assess their survival, larvae were poked with a pipette tip and individuals not responding to the physical stimulation were considered dead. We conducted three independent experiments per pathogen and treatment at different days with larvae from different batches.

Experimental evolution experiment

Treatments and concentrations

In a first step, we determined the IC50 concentrations of (crude) pyoverdines 3A06, 3G07, and s3b09, and the antibiotic ciprofloxacin against all four pathogens. For this, we fitted logistic regressions to the dose-response curves. We used these IC50 values as treatment concentrations during experimental evolution (Table S2). We also mixed different pyoverdines in double and triple combo treatments. In combo treatments, pyoverdine concentrations were equivalent to those of the single treatments, meaning that we divided the single treatment concentrations by two or three. To summarize, the experimental evolution experiment included (i) three single pyoverdine treatments (3A06, 3G07, s3b09), (ii) three double pyoverdine treatments (3A06 and 3G07, 3A06 and s3b09, 3G07 and s3b09), (iii) one triple pyoverdine treatment (3A06, 3G07 and s3b09), and (iv) one ciprofloxacin treatment for *A. baumannii*, *P. aeruginosa* and *S. aureus*. For *K. pneumoniae*, which was only affected by one pyoverdine (3G07), the experiment consisted of one single pyoverdine treatment and one ciprofloxacin treatment.

Plate design and experimental setup

For each pathogen-treatment combination, we included six independently replicating lineages (populations). These replicate populations were arranged along the diagonal of 96-well plates, or at the border of the plates, in such a way that they were surrounded by medium on all sides. This plate layout minimized the chance of cross-contamination and resulted in a total of ten plates (three each for *A. baumannii*, *P. aeruginosa* and *S. aureus* and one for *K. pneumoniae*). Each plate contained two control populations that evolved in plain CAA medium, except for *K. pneumoniae*, for which all six controls were on the same plate. Prior experimental evolution, we prepared batches of media for the entire duration of the experiment. Specifically, all treatments were prepared in CAA medium, then aliquoted into the respective wells of 96-well plates, and all plates were stored at -20 °C. At the start, we grew the pathogens overnight, washed and diluted them as described above, and transferred 2 µL of the diluted pathogens into 200 µL of the thawed 96-well plates. Subsequently, the plates were incubated at 37 °C for 22 hours, shaken at 170 rpm.

Daily transfers

After 22 hours of incubation, we measured growth (OD_{600}) of all evolving lineages with the plate reader. We then diluted the evolving cultures 1:1,000 in CAA medium and added them to a fresh treatment plate thawed from the freezer. After the transfer, the new plates were again incubated at 37 °C and 170 rpm agitation for 22 hours. We added glycerol to the old plates to a final concentration of 25% and stored them at -80 °C. We observed a steady decrease in growth in all *S. aureus* populations, suggesting that we overdiluted these cultures. Consequently, we reduced the dilution to 1:10 from day 4 onwards. Conversely, we observed a study increase in growth for *A. baumannii* and *P. aeruginosa* populations, suggesting that these cultures were not

diluted enough. Consequently, we increased dilution rates to appropriate levels on day 4, day 8, and day 12.

Phenotypic screening of evolved populations

We screened evolved population for improved growth performance relative to the ancestor under pyoverdine treatment, which we took as a proxy for resistance evolution. For this purpose, we thawed the final plates (day 16) of the experimental evolution experiment and transferred 2 µl of all populations to 200 µl of LB or TSB (for *S aureus*) to create overnight cultures in 96-well plates. We further included ancestor cultures of all four species. After incubation for 18 hours at 37 °C and 170 rpm, we diluted overnights 1:1,000 with 0.8% NaCl and subjected all evolved populations to the conditions they had evolved in. Ancestors were simultaneously exposed to the respective treatment conditions. The culturing volume and conditions were the same as during experimental evolution, but this time we incubated the plates in a plate reader, measuring OD_{600} every 15 minutes to obtain growth kinetics. The population screen was repeated twice independently. From the growth kinetics, we first calculated area under the curve (AUC) for each growth curve. AUC values were then scaled relative to the growth of the ancestor in the untreated CAA control medium. For each evolved population, we then calculated the difference in growth in comparison to the mean growth of the ancestor subjected to the same treatment.

Phenotypic screening of evolved clones

To screen for resistant clones within populations, we selected the pathogen populations with the lowest and highest growth difference for each single treatment and for one combination treatment and picked 8 random colonies. We transferred

them to 200 µL LB or TSB (*S. aureus*) in 96-well plates and incubated plates for 18 hours at 37 °C (170 rpm) to create overnight cultures. We followed the same protocol as above for quantifying the difference in growth of evolved and ancestral clones.

Genomic analyses of evolved populations and clones

We sequenced the genomes of the four ancestors, four control populations that had evolved in medium without pyoverdine treatment, and two random clones (out of the eight picked) per population that had received pyoverdine treatment and were used for clonal growth analysis (Figure 6B). We grew the clones and populations in 12 mL LB or TSB (*S. aureus*) at 37 °C and 170 rpm and harvested cultures upon reaching an OD_{600} between 0.8-1 by centrifugation (7,500 rcf, 3 minutes). We washed cultures in 0.8% NaCl and resuspended the pellet in DNA shield buffer (Zymo research). Samples were then sent to MicrobesNG (Birmingham, United Kingdom) for library preparation and sequencing. Whole-genome sequencing was performed on the Illumina NovaSeq6000 platform (Illumina, San Diego, USA) using a 250 bp paired end protocol. Adapter sequences were trimmed using Trimmomatic v0.30[65] with quality cut-off of Q15, and reads were aligned to the closest available reference genome using BWA mem[66]. De novo assemblies were performed using SPAdes v3.7[67] and contigs annotated with Prokka v1.11[68]. Variants were predicted relative to the reference genomes ATCC 19606 (*A. baumannii*), ATCC 13883 (*K. pneumonia*), ATCC 15692 (*P. aeruginosa*) and CP020619.1 (*S. aureus*) using VarScan[69] and annotated using Prokka. For the analysis, we excluded the following variants: (i) coverage < 30 reads; (ii) synonymous mutations; and (iii) mutations that were already present in the ancestor. In cases where we examined only mutations associated with

pyoverdines, we excluded mutations in genes that occurred at least twice in the medium-evolved control populations.

Data analyses

All statistical analyses were performed in R 4.0.2[70] and RStudio version 1.3.1056[71]. We conducted Shapiro-Wilk tests and consulted diagnostic plots to check whether our data (residuals) were normally distributed. For normally distributed data sets, we used linear models and used two-sided tests for all analyses. For non-normally distributed data sets, we used non-parametric rank tests. Specifically, we used ANOVA to test whether chemical properties differ between growth inhibiting and non-inhibiting pyoverdines, in their ferri- versus apo-pyoverdine state. For the *in vitro* dose-response and cytotoxicity experiments, we fitted dose-response curves with either 4- or 5-parameter logistic regressions using the nplr package[72]. Survival analyses were performed using the Cox proportional hazards regression model or the log-rank test (adjusted for multiple comparisons using the Holm method) from the survival package[73]. We used two-sided t-tests, Welch's t-tests, or Wilcoxon tests to compare growth differences between the ancestor and the evolved populations under treatment. To compare growth differences between the ancestor and the evolved clones under treatment, we used one- and two-way ANOVAs.

Acknowledgements

We thank Richard Allen, Dominik Bär, Johanna Giger, Kevin Schiefelbein and Julien Weber for laboratory assistance, and Markus Seeger for insightful discussion. This work was supported by funding from the Swiss National Science Foundation (grant

numbers: 31003A_182499 to RK, PP00P3_144862 and PP00P3_176966 to MP) and a Candoc Grant (Forschungskredit) from the University of Zurich (to MPB).

Authors contributions

VV and RK conceived the project. VV, KR, CC and MPB performed the experiments and analysed experimental results. All authored interpreted the data. VV and RK wrote the manuscript with contributions from all authors.

Competing interests

Authors declare no competing interests.

Data availability statement

All original data associated with this study will be deposited in the Figshare repository upon the acceptance of the manuscript. Bacterial genome sequence data will be deposited at ENA (European nucleotide archive).

References

1. Murray, C. J., Ikuta, K. S., Sharara, F., Swetschinski, L., Aguilar, G. R., Gray, A., Han, C., Bisignano, C., Rao, P., Wool, E., Johnson, S. C., Browne, A. J., Chipeta, M. G., Fell, F., Hackett, S., Haines-Woodhouse, G., Hamadani, B. H. K., Kumaran, E. A. P., McManigal, B., Agarwal, R., Akech, S., Albertson, S., Amuasi, J., Andrews, J., Aravkin, A., Ashley, E., Bailey, F., Baker, S., Basnyat, B., Bekker, A., Bender, R., Bethou, A., Bielicki, J., Boonkasidecha, S., Bukosia, J., Carvalheiro, C., Castañeda-Orjuela, C., Chansamouth, V., Chaurasia, S.,

Chiurchiù, S., Chowdhury, F., Cook, A. J., Cooper, B., Cressey, T. R., Criollo-Mora, E., Cunningham, M., Darboe, S., Day, N. P. J., Luca, M. D., Dokova, K., Dramowski, A., Dunachie, S. J., Eckmanns, T., Eibach, D., Emami, A., Feasey, N., Fisher-Pearson, N., Forrest, K., Garrett, D., Gastmeier, P., Giref, A. Z., Greer, R. C., Gupta, V., Haller, S., Haselbeck, A., Hay, S. I., Holm, M., Hopkins, S., Iregbu, K. C., Jacobs, J., Jarovsky, D., Javanmardi, F., Khorana, M., Kissoon, N., Kobeissi, E., Kostyanev, T., Krapp, F., Krumkamp, R., Kumar, A., Kyu, H. H., Lim, C., Limmathurotsakul, D., Loftus, M. J., Lunn, M., Ma, J., Mturi, N., Munera-Huertas, T., Musicha, P., Mussi-Pinhata, M. M., Nakamura, T., Nanavati, R., Nangia, S., Newton, P., Ngoun, C., Novotney, A., Nwakanma, D., Obiero, C. W., Olivas-Martinez, A., Olliaro, P., Ooko, E., Ortiz-Brizuela, E., Peleg, A. Y., Perrone, C., Plakkal, N., Ponce-de-Leon, A., Raad, M., Ramdin, T., Riddell, A., Roberts, T., Robotham, J. V., Roca, A., Rudd, K. E., Russell, N., Schnall, J., Scott, J. A. G., Shivamallappa, M., Sifuentes-Osornio, J., Steenkeste, N., Stewardson, A. J., Stoeva, T., Tasak, N., Thaiprakong, A., Thwaites, G., Turner, C., Turner, P., Doorn, H. R. van, Velaphi, S., Vongpradith, A., Vu, H., Walsh, T., Waner, S., Wangrangsimakul, T., Wozniak, T., Zheng, P., Sartorius, B., Lopez, A. D., Stergachis, A., Moore, C., Dolecek, C. & Naghavi, M. Global burden of bacterial antimicrobial resistance in 2019: a systematic analysis. *The Lancet* **399,** 629–655 (2022).

2. WHO. 2021 antibacterial agents in clinical and preclinical development: an overview and analysis. (2022). at https://www.who.int/publications-detail-redirect/9789240047655

3. Beyer, P. & Paulin, S. The Antibacterial Research and Development Pipeline Needs Urgent Solutions. *ACS Infect. Dis.* **6,** 1289–1291 (2020).

4. Bell, G. & MacLean, C. The Search for ‘Evolution-Proof’ Antibiotics. *Trends Microbiol.* **26,** 471–483 (2018).
5. Monserrat-Martinez, A., Gambin, Y. & Sierecki, E. Thinking Outside the Bug: Molecular Targets and Strategies to Overcome Antibiotic Resistance. *Int. J. Mol. Sci.* **20,** 1255 (2019).
6. Rezzoagli, C., Granato, E. T. & Kümmerli, R. Harnessing bacterial interactions to manage infections: a review on the opportunistic pathogen Pseudomonas aeruginosa as a case example. *J. Med. Microbiol.* **69,** 147–161 (2020).
7. Bhushan, A., Peters, E. E. & Piel, J. *Entotheonella Bacteria as Source of Sponge-Derived Natural Products: Opportunities for Biotechnological Production*. (Springer International Publishing, 2017).
8. Ghosh, C., Sarkar, P., Issa, R. & Haldar, J. Alternatives to Conventional Antibiotics in the Era of Antimicrobial Resistance. *Trends Microbiol.* **27,** 323–338 (2019).
9. Mei, Y., Chen, Y., Sivaccumar, J. P., An, Z., Xia, N. & Luo, W. Research progress and applications of nanobody in human infectious diseases. *Front. Pharmacol.* **13,** (2022).
10. Rezzoagli, C., Archetti, M., Mignot, I., Baumgartner, M. & Kümmerli, R. Combining antibiotics with antivirulence compounds can have synergistic effects and reverse selection for antibiotic resistance in Pseudomonas aeruginosa. *PLOS Biol.* **18,** (2020).
11. Saeki, E. K., Kobayashi, R. K. T. & Nakazato, G. Quorum sensing system: Target to control the spread of bacterial infections. *Microb. Pathog.* **142,** (2020).

12. Wale, N., Sim, D. G., Jones, M. J., Salathe, R., Day, T. & Read, A. F. Resource limitation prevents the emergence of drug resistance by intensifying within-host competition. *Proc. Natl. Acad. Sci.* **114,** 13774–13779 (2017).
13. Hatcher, H. C., Singh, R. N., Torti, F. M. & Torti, S. V. Synthetic and natural iron chelators: therapeutic potential and clinical use. *Future Med. Chem.* **1,** 1643–1670 (2009).
14. Hug, J. J., Krug, D. & Müller, R. Bacteria as genetically programmable producers of bioactive natural products. *Nat. Rev. Chem.* **4,** 172–193 (2020).
15. Imai, Y., Meyer, K. J., Iinishi, A., Favre-Godal, Q., Green, R., Manuse, S., Caboni, M., Mori, M., Niles, S., Ghiglieri, M., Honrao, C., Ma, X., Guo, J. J., Makriyannis, A., Linares-Otoya, L., Böhringer, N., Wuisan, Z. G., Kaur, H., Wu, R., Mateus, A., Typas, A., Savitski, M. M., Espinoza, J. L., O'Rourke, A., Nelson, K. E., Hiller, S., Noinaj, N., Schäberle, T. F., D'Onofrio, A. & Lewis, K. A new antibiotic selectively kills Gram-negative pathogens. *Nature* **576,** 459–464 (2019).
16. Ling, L. L., Schneider, T., Peoples, A. J., Spoering, A. L., Engels, I., Conlon, B. P., Mueller, A., Schäberle, T. F., Hughes, D. E., Epstein, S., Jones, M., Lazarides, L., Steadman, V. A., Cohen, D. R., Felix, C. R., Fetterman, K. A., Millett, W. P., Nitti, A. G., Zullo, A. M., Chen, C. & Lewis, K. A new antibiotic kills pathogens without detectable resistance. *Nature* **517,** 455–459 (2015).
17. Butaitė, E., Baumgartner, M., Wyder, S. & Kümmerli, R. Siderophore cheating and cheating resistance shape competition for iron in soil and freshwater Pseudomonas communities. *Nat. Commun.* **8,** 414 (2017).
18. Deveau, A., Gross, H., Palin, B., Mehnaz, S., Schnepf, M., Leblond, P., Dorrestein, P. C. & Aigle, B. Role of secondary metabolites in the interaction

between Pseudomonas fluorescens and soil microorganisms under iron-limited conditions. *FEMS Microbiol. Ecol.* **92,** (2016).

19. Hider, R. C. & Kong, X. Chemistry and biology of siderophores. *Nat. Prod. Rep.* **27,** 637–657 (2010).
20. Figueiredo, A. R. T., Özkaya, Ö., Kümmerli, R. & Kramer, J. Siderophores drive invasion dynamics in bacterial communities through their dual role as public good versus public bad. *Ecol. Lett.* **25,** 138–150 (2022).
21. Gu, S., Wei, Z., Shao, Z., Friman, V.-P., Cao, K., Yang, T., Kramer, J., Wang, X., Li, M., Mei, X., Xu, Y., Shen, Q., Kümmerli, R. & Jousset, A. Competition for iron drives phytopathogen control by natural rhizosphere microbiomes. *Nat. Microbiol.* **5,** 1002–1010 (2020).
22. Lee, W., van Baalen, M. & Jansen, V. A. A. An evolutionary mechanism for diversity in siderophore-producing bacteria. *Ecol. Lett.* **15,** 119–125 (2012).
23. Niehus, R., Picot, A., Oliveira, N. M., Mitri, S. & Foster, K. R. The evolution of siderophore production as a competitive trait. *Evolution* **71,** 1443–1455 (2017).
24. Visca, P., Imperi, F. & Lamont, I. L. Pyoverdine siderophores: from biogenesis to biosignificance. *Trends Microbiol.* **15,** 22–30 (2007).
25. Bonneau, A., Roche, B. & Schalk, I. J. Iron acquisition in Pseudomonas aeruginosa by the siderophore pyoverdine: an intricate interacting network including periplasmic and membrane proteins. *Sci. Rep.* **10,** 120 (2020).
26. Cornelis, P., Tahrioui, A., Lesouhaitier, O., Bouffartigues, E., Feuilloley, M., Baysse, C. & Chevalier, S. High affinity iron uptake by pyoverdine in Pseudomonas aeruginosa involves multiple regulators besides Fur, PvdS, and FpvI. *BioMetals* (2022).

27. Meyer, J.-M., Gruffaz, C., Raharinosy, V., Bezverbnaya, I., Schäfer, M. & Budzikiewicz, H. Siderotyping of fluorescent Pseudomonas: molecular mass determination by mass spectrometry as a powerful pyoverdine siderotyping method. *BioMetals* **21,** 259–271 (2008).
28. Rehm, K., Vollenweider, V., Kümmerli, R. & Bigler, L. A comprehensive method to elucidate pyoverdines produced by fluorescent Pseudomonas spp. by UHPLC-HR-MS/MS. *Anal. Bioanal. Chem.* **414,** 2671–2685 (2022).
29. Meyer & Abdallah, M. A. The Fluorescent Pigment of Pseudomonas fluorescens: Biosynthesis, Purification and Physicochemical Properties. *Microbiology* **107,** 319–328 (1978).
30. Butaitė, E., Kramer, J., Wyder, S. & Kümmerli, R. Environmental determinants of pyoverdine production, exploitation and competition in natural Pseudomonas communities. *Environ. Microbiol.* **20,** 3629–3642 (2018).
31. Butaitė, E., Kramer, J. & Kümmerli, R. Local adaptation, geographical distance and phylogenetic relatedness: Assessing the drivers of siderophore-mediated social interactions in natural bacterial communities. *J. Evol. Biol.* **34,** 1266–1278 (2021).
32. Kramer, J., López Carrasco, M. Á. & Kümmerli, R. Positive linkage between bacterial social traits reveals that homogeneous rather than specialised behavioral repertoires prevail in natural Pseudomonas communities. *FEMS Microbiol. Ecol.* **96,** (2020).
33. Meyer, J.-M. Pyoverdines: pigments, siderophores and potential taxonomic markers of fluorescent Pseudomonas species. *Arch. Microbiol.* **174,** 135–142 (2000).

34. Rehm, K., Vollenweider, V., Kümmerli, R. & Bigler, L. Rapid identification of pyoverdines of fluorescent Pseudomonas spp. by UHPLC-IM-MS. *BioMetals* **36,** 19–34 (2023).

35. Meyer, J.-M., Stintzi, A., De Vos, D., Cornelis, P., Tappe, R., Taraz, K. & Budzikiewicz, H. 1997. Use of Siderophores to Type Pseudomonads: The Three Pseudomonas Aeruginosa Pyoverdine Systems. *Microbiology* **143,** 35–43 (1997).

36. Budzikiewicz, H., Schäfer, M., Fernández, D. U., Matthijs, S. & Cornelis, P. Characterization of the chromophores of pyoverdins and related siderophores by electrospray tandem mass spectrometry. *BioMetals* **20,** 135–144 (2007).

37. Nadal-Jimenez, P., Koch, G., Reis, C. R., Muntendam, R., Raj, H., Jeronimus-Stratingh, C. M., Cool, R. H. & Quax, W. J. PvdP Is a Tyrosinase That Drives Maturation of the Pyoverdine Chromophore in Pseudomonas aeruginosa. *J. Bacteriol.* **196,** 2681–2690 (2014).

38. Harris, W. R., Carrano, C. J., Cooper, S. R., Sofen, S. R., Avdeef, A. E., McArdle, J. V. & Raymond, K. N. Coordination chemistry of microbial iron transport compounds. 19. Stability constants and electrochemical behavior of ferric enterobactin and model complexes. *J. Am. Chem. Soc.* **101,** 6097–6104 (1979).

39. Ghysels, B., Dieu, B. T. M., Beatson, S. A., Pirnay, J.-P., Ochsner, U. A., Vasil, M. L. & Cornelis, P. 2004. FpvB, an alternative type I ferripyoverdine receptor of Pseudomonas aeruginosa. *Microbiology* **150,** 1671–1680 (2004).

40. González, J., Salvador, M., Özkaya, Ö., Spick, M., Reid, K., Costa, C., Bailey, M. J., Avignone Rossa, C., Kümmerli, R. & Jiménez, J. I. Loss of a pyoverdine secondary receptor in Pseudomonas aeruginosa results in a fitter strain suitable for population invasion. *ISME J.* **15,** 1330–1343 (2021).

41. Sexton, D. J., Glover, R. C., Loper, J. E. & Schuster, M. Pseudomonas protegens Pf-5 favours self-produced siderophore over free-loading in interspecies competition for iron. *Environ. Microbiol.* **19,** 3514–3525 (2017).

42. Ménard, G., Rouillon, A., Ghukasyan, G., Emily, M., Felden, B. & Donnio, P.-Y. Galleria mellonella Larvae as an Infection Model to Investigate sRNA-Mediated Pathogenesis in Staphylococcus aureus. *Front. Cell. Infect. Microbiol.* **11,** (2021).

43. Bohac, T. J., Fang, L., Giblin, D. E. & Wencewicz, T. A. Fimsbactin and Acinetobactin Compete for the Periplasmic Siderophore Binding Protein BauB in Pathogenic Acinetobacter baumannii. *ACS Chem. Biol.* **14,** 674–687 (2019).

44. Shapiro, J. A. & Wencewicz, T. A. Acinetobactin Isomerization Enables Adaptive Iron Acquisition in Acinetobacter baumannii through pH-Triggered Siderophore Swapping. *ACS Infect. Dis.* **2,** 157–168 (2016).

45. Sheldon, J. R. & Skaar, E. P. Acinetobacter baumannii can use multiple siderophores for iron acquisition, but only acinetobactin is required for virulence. *PLOS Pathog.* **16,** (2020).

46. Hammer, N. D. & Skaar, E. P. Molecular Mechanisms of Staphylococcus aureus Iron Acquisition. *Annu. Rev. Microbiol.* **65,** 129–147 (2011).

47. Cassat, J. E. & Skaar, E. P. Iron in Infection and Immunity. *Cell Host Microbe* **13,** 509–519 (2013).

48. Skaar, E. P. The Battle for Iron between Bacterial Pathogens and Their Vertebrate Hosts. *PLOS Pathog.* **6,** (2010).

49. Döring, G., Pfestorf, M., Botzenhart, K. & Abdallah, M. A. Impact of proteases on iron uptake of Pseudomonas aeruginosa pyoverdin from transferrin and lactoferrin. *Infect. Immun.* **56,** 291–293 (1988).

50. Cox, C. D. Role of pyocyanin in the acquisition of iron from transferrin. *Infect. Immun.* **52,** 263–270 (1986).

51. Wolz, C., Hohloch, K., Ocaktan, A., Poole, K., Evans, R. W., Rochel, N., Albrecht-Gary, A. M., Abdallah, M. A. & Döring, G. Iron release from transferrin by pyoverdin and elastase from Pseudomonas aeruginosa. *Infect. Immun.* **62,** 4021–4027 (1994).

52. Kang, D. & Kirienko, N. V. An In Vitro Cell Culture Model for Pyoverdine-Mediated Virulence. *Pathogens* **10,** 9 (2021).

53. Kirienko, N. V., Kirienko, D. R., Larkins-Ford, J., Wählby, C., Ruvkun, G. & Ausubel, F. M. Pseudomonas aeruginosa Disrupts Caenorhabditis elegans Iron Homeostasis, Causing a Hypoxic Response and Death. *Cell Host Microbe* **13,** 406–416 (2013).

54. Pita-Grisanti, V., Chasser, K., Sobol, T. & Cruz-Monserrate, Z. Understanding the Potential and Risk of Bacterial Siderophores in Cancer. *Front. Oncol.* **12,** (2022).

55. Peek, M. E., Bhatnagar, A., McCarty, N. A. & Zughaier, S. M. Pyoverdine, the Major Siderophore in Pseudomonas aeruginosa, Evades NGAL Recognition. *Interdiscip. Perspect. Infect. Dis.* **2012,** (2012).

56. Rezzoagli, C., Wilson, D., Weigert, M., Wyder, S. & Kümmerli, R. Probing the evolutionary robustness of two repurposed drugs targeting iron uptake in Pseudomonas aeruginosa. *Evol. Med. Public Health* **2018,** 246–259 (2018).

57. Sommer, M. O. A., Munck, C., Toft-Kehler, R. V. & Andersson, D. I. Prediction of antibiotic resistance: time for a new preclinical paradigm? *Nat. Rev. Microbiol.* **15,** 689–696 (2017).

58. Imperi, F., Massai, F., Facchini, M., Frangipani, E., Visaggio, D., Leoni, L., Bragonzi, A. & Visca, P. Repurposing the antimycotic drug flucytosine for

suppression of Pseudomonas aeruginosa pathogenicity. *Proc. Natl. Acad. Sci.* **110,** 7458–7463 (2013).

59. Kelson, A. B., Carnevali, M. & Truong-Le, V. Gallium-based anti-infectives: targeting microbial iron-uptake mechanisms. *Curr. Opin. Pharmacol.* **13,** 707–716 (2013).

60. Schalk, I. J. & Mislin, G. L. A. Bacterial Iron Uptake Pathways: Gates for the Import of Bactericide Compounds. *J. Med. Chem.* **60,** 4573–4576 (2017).

61. Thompson, M. G., Corey, B. W., Si, Y., Craft, D. W. & Zurawski, D. V. Antibacterial Activities of Iron Chelators against Common Nosocomial Pathogens. *Antimicrob. Agents Chemother.* **56,** 5419–5421 (2012).

62. Yang, J., Long, H., Hu, Y., Feng, Y., McNally, A. & Zong, Z. Klebsiella oxytoca Complex: Update on Taxonomy, Antimicrobial Resistance, and Virulence. *Clin. Microbiol. Rev.* **35,** (2021).

63. Cunrath, O., Geoffroy, V. A. & Schalk, I. J. Metallome of Pseudomonas aeruginosa: a role for siderophores. *Environ. Microbiol.* **18,** 3258–3267 (2016).

64. Sprouffske, K. & Wagner, A. Growthcurver: An R package for obtaining interpretable metrics from microbial growth curves. *BMC Bioinformatics* **17,** 172 (2016).

65. Bolger, A. M., Lohse, M. & Usadel, B. Trimmomatic: a flexible trimmer for Illumina sequence data. *Bioinformatics* **30,** 2114–2120 (2014).

66. Li, H. & Durbin, R. Fast and accurate short read alignment with Burrows–Wheeler transform. *Bioinformatics* **25,** 1754–1760 (2009).

67. Bankevich, A., Nurk, S., Antipov, D., Gurevich, A., Dvorkin, M., Kulikov, A. S., Lesin, V. M., Nikolenko, S. I., Pham, S., Prjibelski, A. D., Pyshkin, A. V., Sirotkin, A., Vyahhi, N., Tesler, G., Alekseyev, M. A. & Pevzner, P. A. SPAdes: A New

Genome Assembly Algorithm and Its Applications to Single-Cell Sequencing. *J. Comput. Biol.* (2012).

68. Seemann, T. Prokka: rapid prokaryotic genome annotation. *Bioinformatics* **30,** 2068–2069 (2014).
69. Koboldt, D. C., Zhang, Q., Larson, D. E., Shen, D., McLellan, M. D., Lin, L., Miller, C. A., Mardis, E. R., Ding, L. & Wilson, R. K. VarScan 2: Somatic mutation and copy number alteration discovery in cancer by exome sequencing. *Genome Res.* **22,** 568–576 (2012).
70. R Core Team. R: A language and environment for statistical computing. R Foundation for Statistical Computing, Vienna, Austria. (2020).
71. RStudio Team. RStudio: Integrated Development Environment for R. RStudio. (2020).
72. Commo, F. & Bot, B. nplr: N-Parameter Logistic Regression. R package version 0.1-7. (2016).
73. Therneau, T. _A Package for Survival Analysis in R_. (2020). at https://CRAN.R-project.org/package=survival